



**NAVAL
POSTGRADUATE
SCHOOL**

MONTEREY, CALIFORNIA

THESIS

**ALUMINUM REACTIVE MATERIAL WARHEAD
CASINGS**

by

Daniel A. Kotei

December 2018

Thesis Advisor:
Second Reader:

Joseph P. Hooper
Troy Ansell

Approved for public release. Distribution is unlimited.

THIS PAGE INTENTIONALLY LEFT BLANK

REPORT DOCUMENTATION PAGE			<i>Form Approved OMB No. 0704-0188</i>	
Public reporting burden for this collection of information is estimated to average 1 hour per response, including the time for reviewing instruction, searching existing data sources, gathering and maintaining the data needed, and completing and reviewing the collection of information. Send comments regarding this burden estimate or any other aspect of this collection of information, including suggestions for reducing this burden, to Washington headquarters Services, Directorate for Information Operations and Reports, 1215 Jefferson Davis Highway, Suite 1204, Arlington, VA 22202-4302, and to the Office of Management and Budget, Paperwork Reduction Project (0704-0188) Washington, DC 20503.				
1. AGENCY USE ONLY (Leave blank)		2. REPORT DATE December 2018	3. REPORT TYPE AND DATES COVERED Master's thesis	
4. TITLE AND SUBTITLE ALUMINUM REACTIVE MATERIAL WARHEAD CASINGS			5. FUNDING NUMBERS RPLP7	
6. AUTHOR(S) Daniel A. Kotei				
7. PERFORMING ORGANIZATION NAME(S) AND ADDRESS(ES) Naval Postgraduate School Monterey, CA 93943-5000			8. PERFORMING ORGANIZATION REPORT NUMBER	
9. SPONSORING / MONITORING AGENCY NAME(S) AND ADDRESS(ES) N/A			10. SPONSORING / MONITORING AGENCY REPORT NUMBER	
11. SUPPLEMENTARY NOTES The views expressed in this thesis are those of the author and do not reflect the official policy or position of the Department of Defense or the U.S. Government.				
12a. DISTRIBUTION / AVAILABILITY STATEMENT Approved for public release. Distribution is unlimited.			12b. DISTRIBUTION CODE A	
13. ABSTRACT (maximum 200 words) Pure aluminum metal manufactured using Cold Isostatic Press (CIP) bears the properties of Structural Reactive Material (SRM) and has the capacity to increase lethality due to the continuous combustion of the fragments after explosion. This thesis focuses on the enhanced lethality and reactivity produced by replacing conventional warhead casings with SRM aluminum manufactured using CIP. Pure Al SRM is totally unclassified and can be studied by academic groups, other NATO countries, and so on to study the properties of SRM without classification issues. Mechanical and fragmentation analysis were conducted on three Al SRMs. H2(37%wt)/H15(63%wt), H15(90%wt)/Sn(10%wt) and pure H15. H15 is eventually selected to produce the first set of explosive casings for testing. Two types of Al H15 SRM casings with average mass to charge (M/C) ratio of 1.86 and 2.82 at 5% porosity were made for testing. Explosive experiment is then conducted in a cylindrical chamber to determine ballistic properties and reactivity of CIP H15 SRM cases compared to conventional 6061 aluminum casing.				
14. SUBJECT TERMS reactive materials, fragmentation, ballistic properties, combustion, lethality			15. NUMBER OF PAGES 89	
			16. PRICE CODE	
17. SECURITY CLASSIFICATION OF REPORT Unclassified	18. SECURITY CLASSIFICATION OF THIS PAGE Unclassified	19. SECURITY CLASSIFICATION OF ABSTRACT Unclassified	20. LIMITATION OF ABSTRACT UU	

THIS PAGE INTENTIONALLY LEFT BLANK

Approved for public release. Distribution is unlimited.

ALUMINUM REACTIVE MATERIAL WARHEAD CASINGS

Daniel A. Kotei
Lieutenant, United States Navy
BS, University of North Florida, 2012

Submitted in partial fulfillment of the
requirements for the degree of

MASTER OF SCIENCE IN MECHANICAL ENGINEERING

from the

**NAVAL POSTGRADUATE SCHOOL
December 2018**

Approved by: Joseph P. Hooper
Advisor

Troy Ansell
Second Reader

Garth V. Hobson
Chair, Department of Mechanical and Aerospace Engineering

THIS PAGE INTENTIONALLY LEFT BLANK

ABSTRACT

Pure aluminum metal manufactured using Cold Isostatic Press (CIP) bears the properties of Structural Reactive Material (SRM) and has the capacity to increase lethality due to the continuous combustion of the fragments after explosion. This thesis focuses on the enhanced lethality and reactivity produced by replacing conventional warhead casings with SRM aluminum manufactured using CIP. Pure Al SRM is totally unclassified and can be studied by academic groups, other NATO countries, and so on to study the properties of SRM without classification issues. Mechanical and fragmentation analysis were conducted on three Al SRMs. H2(37% wt)/H15(63% wt), H15(90% wt)/Sn(10% wt) and pure H15. H15 is eventually selected to produce the first set of explosive casings for testing. Two types of Al H15 SRM casings with average mass to charge (M/C) ratio of 1.86 and 2.82 at 5% porosity were made for testing. Explosive experiment is then conducted in a cylindrical chamber to determine ballistic properties and reactivity of CIP H15 SRM cases compared to conventional 6061 aluminum casing.

THIS PAGE INTENTIONALLY LEFT BLANK

TABLE OF CONTENTS

I.	INTRODUCTION.....	1
II.	EXPERIMENTAL METHODOLOGY.....	3
	A. COLD ISOSTATIC PRESS.....	3
	B. MACHINING.....	7
	C. SPLIT HOPKINSON BAR EXPERIMENT.....	8
	D. SOUND SPEED TEST.....	11
	E. FRAGMENTATION ANALYSIS.....	12
	F. EXPLOSIVE LAUNCH EXPERIMENT.....	13
III.	RESULTS AND DISCUSSION.....	17
	A. MECHANICAL PROPERTIES.....	17
	1. Density and Porosity.....	17
	2. Longitudinal and Shear Sound Speed.....	21
	3. Moduli.....	22
	B. FRAGMENTATION ANALYSIS.....	28
	C. EXPLOSIVE LAUNCH.....	33
IV.	CONCLUSION AND FUTURE WORK.....	35
	APPENDIX A. COLD ISOSTATIC PRESS STANDARD OPERATING PROCEDURE.....	37
	A. REQUIRED MATERIALS AND EQUIPMENT.....	37
	B. POWDER PREPARATION.....	38
	C. PARTS OF THE COLD ISOSTATIC PRESS.....	42
	D. PRESSING PROCEDURE.....	43
	APPENDIX B. SPLIT HOPKINSON PRESSURE BAR STANDARD OPERATING PROCEDURE.....	49
	APPENDIX C. MATLAB CODE.....	51
	A. PACKING EFFICIENCY PLOT MATLAB CODE.....	51
	B. DENSITY PLOT MATLAB CODES.....	52
	C. STRESS / STRAIN PLOT MATLAB CODES.....	53
	D. BRAZILIAN FORCE / STRAIN PLOT MATLAB CODES.....	57

E. PROBABILITY DENSITY FUNCTION AND CUMULATIVE DISTRIBUTION FUNCTION MATLAB CODE	58
LIST OF REFERENCES	67
INITIAL DISTRIBUTION LIST	69

LIST OF FIGURES

Figure 1.	AIP CP 360 Cold Isostatic Press.....	3
Figure 2.	Pre-existing mold and pressed specimen	3
Figure 3.	Molds components	4
Figure 4.	SEM in SE imaging mode at 500X magnification of powders used; H2 (top left), H15 (top right) and Sn (bottom)	5
Figure 5.	Packing efficiency with various Valimet aluminum powders, assuming the fine particles were H2	6
Figure 6.	SEM in SE imaging mode at 500X magnification for CIPed H2/H15 (left), CIPed H15 (right)	6
Figure 7.	SEM in SE imaging mode at 500X magnification for H15/Sn.....	7
Figure 8.	Pressed H15 cases, M/C 3(left) and M/C 2 (right)	7
Figure 9.	Finished H15 casings after lathing.....	8
Figure 10.	Split Hopkinson compression test.....	8
Figure 11.	Split Hopkinson Dynamic Brazilian test set up	11
Figure 12.	Sound speed test samples. H2/H15(left), H15/Sn (right)	11
Figure 13.	Tektronix DPO 71254 Digital Phosphor Oscilloscope (left) and Olympus Model 5072PR Pulser/Receiver (right).....	11
Figure 14.	Schematic and image of the 0.5” Single Stage Gas Gun	13
Figure 15.	CIPed H15 Al cases M/C 2 (top) and M/C 3 (bottom).....	14
Figure 16.	Al 6061 M/C 2 (top) and M/C 3 (bottom).	14
Figure 17.	Charge assembly consisting of Al H15 case, 6061 Al endcaps, PLX explosive fill, and RP 80 detonator.....	15
Figure 18.	Snow filled HOG chamber for soft catch	15
Figure 19.	Charge assembly hanging in snow cavity.....	16

Figure 20.	Density variations of H15 cylinders used in experiment	18
Figure 21.	Density variations H15 cases used in experiment.....	18
Figure 22.	Density variations of H2/H15 cylinders used in experiment	19
Figure 23.	Density variations H15/Sn cylinders used in experiment	19
Figure 24.	CIP hydrostatic pressure distribution on cylinder (left) and case (right).	20
Figure 25.	Stress/strain plot H2/H15 and H15/Sn (moderate strain rate)	22
Figure 26.	Stress/strain plot H2/H15, H15/Sn and H15 (moderate strain rate).....	23
Figure 27.	Stress/strain plot H2/H15 and H15/Sn (high strain rate)	23
Figure 28.	Stress/strain plot H2/H15, H15/Sn and H15 (high strain rate)	24
Figure 29.	Dynamic Brazilian test 1, H2/H15 and H15/Sn.....	24
Figure 30.	Dynamic Brazilian test 2, H2/H15 and H15/Sn.....	25
Figure 31.	Dynamic Brazilian test 3, H2/H15, H15/Sn and H15	25
Figure 32.	Frame captured from H15 Dynamic Brazilian test (left), DIC E_{yy} strain image (right) just before the tensile crack opens.	27
Figure 33.	Frame captured from H15 Dynamic Brazilian test (left), DIC E_{yy} strain image (right) just after the tensile crack opens.	27
Figure 34.	Fragment distributions from pure H15 projectiles. Note that the data shown in black is for a projectile that tilted prior to impact.	30
Figure 35.	Fragment distributions from projectiles made from an H15/H2 mixture.	30
Figure 36.	Fragment distributions for the H15/Sn10 projectiles.....	31
Figure 37.	Cumulative distribution functions of all three materials at comparable velocities, showing similarities in the characteristic particle size.	31
Figure 38.	H15 light gas gun fragments at 565 m/s	32
Figure 39.	H2/H15 light gas gun fragments at 563 m/s	32

Figure 40.	H15/Sn light gas gun fragments at 550 m/s	32
Figure 41.	CDF and PDF of H15 and T6 cases from explosive launch experiments at RMSL	33
Figure 42.	Images of all the fragments sieved out by particle size	34

THIS PAGE INTENTIONALLY LEFT BLANK

LIST OF TABLES

Table 1.	Aluminum RM powder size and concentration	4
Table 2.	Moderate strain rate (19.05mm diameter striker bar)	9
Table 3.	High strain rate (9.525 mm diameter striker bar)	10
Table 4.	Dynamic Brazilian test samples.....	10
Table 5.	Single stage gas gun sample data.....	12
Table 6.	HOG detonation sample data	14
Table 7.	Density and M/C ratio of CIPed cases	17
Table 8.	Average densities and porosities of Al RMs.....	20
Table 9.	H15/Sn sound speed test data ($t = 7.4\text{mm}$)	21
Table 10.	H2/H15 sound speed test data ($t = 6.5\text{mm}$)	22
Table 11.	Mechanical properties of Al RMs compared to Al 6061	26
Table 12.	Fragment distribution fit parameters.....	29

THIS PAGE INTENTIONALLY LEFT BLANK

LIST OF ACRONYMS AND ABBREVIATIONS

Al	aluminum
C	Celsius
cc	cubic centimeter
CDF	Cumulative distributive function
CIP	Cold Isostatic Press
cm	centimeter
CYL	cylinder
d_{50}	median diameter
g	grams
HDRM	High Density Reactive Material
L/D	length to diameter
M/C	mass to charge ratio
m/s	meters per second
M-7	Matsys #7
mm	millimeter
NPS	Navy Postgraduate School
PDF	Probability density function
RM	Reactive Materials
RM	reactive material
SE	secondary electrons
SEM	scanning electron microscope
SHPB	Split Hopkinson pressure bar
Sn	tin
SOP	standard operating procedure
T6	aluminum 6061
TMD	Theoretical Maximum Density
USN	U.S. Navy
μm	micrometer
μs	microsecond

THIS PAGE INTENTIONALLY LEFT BLANK

ACKNOWLEDGMENTS

The author would like to thank Dr. Joseph Hooper from the Naval Postgraduate School for his continual guidance and instruction with this thesis; Mr. Jacob Kline for assistance in sample analysis and testing; and Mr. Steven Jacobs for allowing me full access to his machine shop. Finally, I want to thank the U.S. Navy for giving me the opportunity to earn my master's degree in mechanical engineering at the Naval Postgraduate School.

THIS PAGE INTENTIONALLY LEFT BLANK

I. INTRODUCTION

Reactive materials (RM) are broadly defined as energetic compounds that will release significant amounts of combustion energy after impact or dynamic loading. They are normally non-detonable, and in the Navy the majority of RMs rely on metal combustion to produce energy. These metallic reactive materials have heats of combustion in air that exceed that of traditional explosives, and can significantly increase lethality for target sets where a slower combustion can still produce damage. Previous research in reactive materials at the Naval Postgraduate School and the broader Navy has been primarily focused on High Density Reactive Materials (HDRM), which are brittle metallic composites with high densities, high enthalpies of combustion, and high compression strengths.

Most metal RMs require significant fragmentation of the material in order to create fine, pyrophoric debris that can begin combusting. As these compounds are often brittle and granular, it has been challenging to study the fine debris produced by an RM following impact or explosive launch. This thesis focuses on manufacturing, characterization, and fragmentation testing of a prototypical aluminum reactive material that provides a baseline for an unclassified study of the broader class of RMs. The aluminum materials produced here are also similar to other low-density RMs currently under study by Defense Threat Reduction Agency (DTRA) and the Air Force.

Mechanical and fragmentation analysis was conducted on three variations of aluminum RMs; H2/H15, pure H15, and H15/Sn. Explosive testing on pure H15 casings was also used to provide data on fragmentation and combustion energy release for comparison with future modeling efforts.

Materials for this thesis were manufactured via a cold-isostatic pressing (CIP) followed by annealing or sintering. Samples of each aluminum RM variation were analyzed with quasistatic mechanical testing as well as microscopy to determine the degree of consolidation and remaining porosity. Samples were analyzed under dynamic loading using

a split Hopkinson pressure bar to determine both compressive strength as well as an estimate for tensile failure stress. Impact fragmentation experiments on a 0.5" gas gun were used to compare the fragment pattern of each material to previous data on similar RMs. Finally, new molds were developed and tested in order to produce controlled cylindrical cases of aluminum RM that were suitable for explosive testing. A process was developed for creating aluminum cases with a case mass M to explosive charge mass C ratio of $M/C=2$ and 3. These cases were filled with sensitized nitromethane and detonated in a confined chamber filled with a snow medium. Initial results on this explosive launch and recovery are reported.

The three variations of aluminum RMs tested were very similar in strength and other mechanical properties. H15 is found to have slightly less porosity than H2/H15 but this did not translate into superior yield and tensile strength. The addition of tin as a liquid-sintering additive increased the density and improved porosity but also did not add significant strength to the RM. Impact fragmentation of all three materials against thin perforation targets show that their fragment pattern is similar and is well-fit by a combined power-law and Mott distribution similar to what has been used for other reactive materials. Overall it was determined that pure H15 was easily CIPed and machined, making it the best option out of the three to make the initial cases for explosive charge test. Cases were filled with sensitized nitromethane and detonated in a snow chamber, allowing for complete fragment recovery of the H15 material following explosive launch.

II. EXPERIMENTAL METHODOLOGY

A. COLD ISOSTATIC PRESS

Cold isostatic pressing was used to consolidate all samples discussed in this thesis. The first step in the CIP process is designing an elastomer mold that will yield the required dimensions for the metal casings, accounting for material shrinkage during pressing. The AIP CP360 CIP in Figure 1 was used to press a cylinder of pure H15 aluminum at 380 MPa using a pre-existing mold from Trexler Rubber shown in Figure 2. The volumetric shrinkage rate is then calculated using the volume of the mold and the volume of the cylinder.



Figure 1. AIP CP 360 Cold Isostatic Press



Figure 2. Pre-existing mold and pressed specimen

For the explosive testing, controlled cylindrical samples were required. For this, a stainless-steel mandrel of 25.4 mm inside diameter was used in conjunction with a multi-piece 40 durometer rubber mold. Using the estimated shrink rate from simple cylinders, two molds were designed with inside diameters of 38.1 mm and 44.45 mm as shown in Figure 3. The goal was to achieve M/C ratios between 2 and 3 for 76.2 mm length cases. An SOP for the AIP CP360 CIP is given in Appendix A.

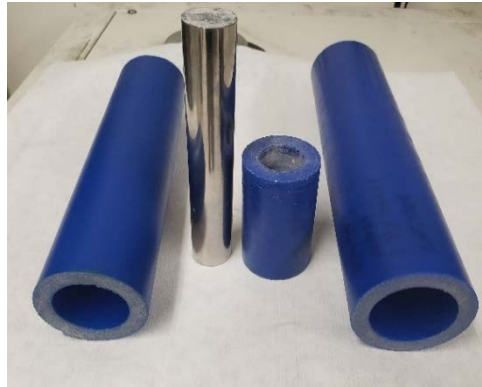


Figure 3. Molds components

The next step in the CIP process is powder selection and characterization. Particle size, morphology and distribution contributes significantly to the quality of the final product. Three variations of aluminum RMs in Table 1 are considered in this thesis. The aluminum powders are products of Valimet, Inc and the tin powder is from US Research Nanomaterials, Inc. All powders are gas-atomized and are generally spherical with an average particle size d_{50} given in Table 1.

Table 1. Aluminum RM powder size and concentration

	H15	H2 / H15	H15 / Sn
$d_{50}(\mu\text{m})$	20	3.5/20	20/20
Concentration (wt%)	100	37/63	90/10

Numerous studies in Powder Metallurgy (PM) have shown that the best way to improve powder packing density is to use bimodal powder mixtures at a fine powder volume fraction between 0.2–0.4 [1]. Figure 4 is the SEM images of the powders used in this experiment. H2/H15 mixture was selected to examine if this would provide superior compaction or other properties desirable for a reactive material. An empirical formula which considered the particle size ratio, the volume fraction of the powders, and their initial packing efficiencies [2] was used to determine the optimal mixing for common aluminum size designations available from Valimet. H2 is selected as the fine powder, and mixed with H3, H5, H10, H15, H30, H50, H60 and H90. The resulting MATLAB plot is illustrated in Figure 5 (MATLAB code in Appendix C). Highest packing density observed between H2 and H15 at 37wt% and 63wt%, respectively. For all data shown, the fine particles were assumed to be Valimet H2, which has a mean particle size of 3.5 microns.

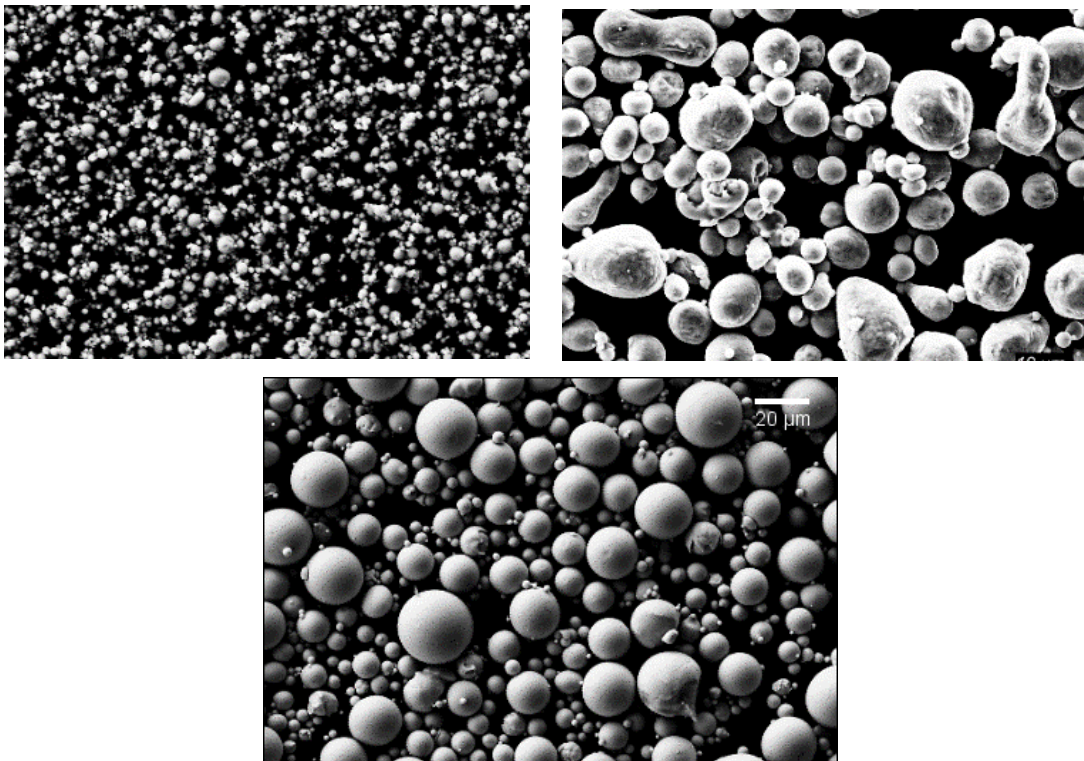


Figure 4. SEM in SE imaging mode at 500X magnification of powders used; H2 (top left), H15 (top right) and Sn (bottom)



Figure 5. Packing efficiency with various Valimet aluminum powders, assuming the fine particles were H2

Two additional aluminum powder mixtures were considered as part of this thesis. Pure H15 was selected because it provides a logical baseline for analysis and was found to produce robust, machinable samples. The third variation included 10% tin to analyze a binder which allowed liquid phase sintering. Pure aluminum traditionally does not sinter well, but previous literature results showed evidence of good consolidation when adding tin as a binder. All powder mixtures were weighed, mixed in a SPEX sample prep high energy ball mill with no media for 30 s, and CIPed in a rubber model at 380 MPa for 30 minutes. Figures 6 and 7 are SEM images showing the deformation of the powders after CIPing. The white aggressively deformed powder in Figure 7 is tin.

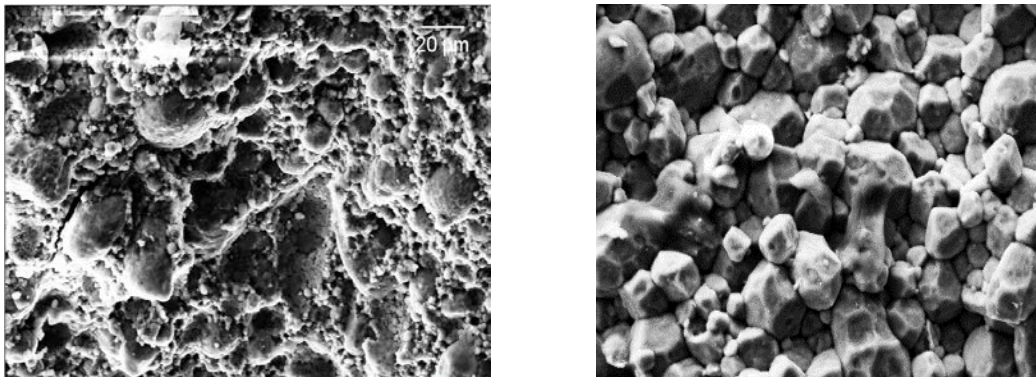


Figure 6. SEM in SE imaging mode at 500X magnification for CIPed H2/H15 (left), CIPed H15 (right)

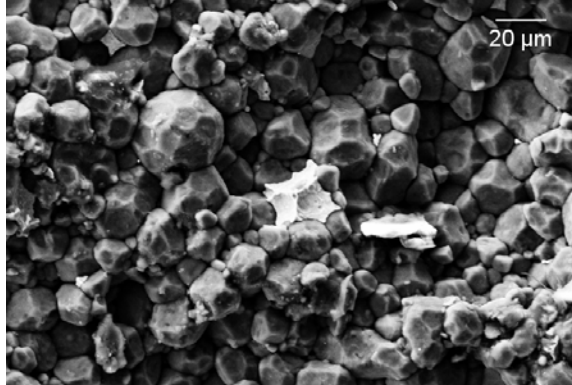


Figure 7. SEM in SE imaging mode at 500X magnification for H15/Sn

B. MACHINING

The molds are intentionally designed to produce parts that are slightly oversized because the CIPed products are usually warped and flared at the ends as can be seen in Figure 8. Aluminum is generally one of the most easily machined metals available, but CIP aluminum is very brittle and very complex to machine. Using a precision lathe in the NPS machine shop the casings were carefully machined at varying speeds and feeds ranging from 250 rpm to 700 rpm and 0.05 mm/rev to 0.10 mm/rev. Figure 9 shows two of the machined H15 RM casings.



Figure 8. Pressed H15 cases, M/C 3(left) and M/C 2 (right)



Figure 9. Finished H15 casings after lathing

C. SPLIT HOPKINSON BAR EXPERIMENT

Split Hopkinson pressure bar (SHPB) testing is an optimal way to quickly determine the strength and ductility of solids in dynamic compression. Variations in the Split Hopkinson bar configuration also makes it possible to determine different properties of the material being investigated. Generally, a cylindrical sample is wedged between the incident bar and the transmission bar. A striker bar launched by compressed air strikes the incident bar generating an elastic wave pulse. The wave propagates through the incident bar and a portion of it is reflected at the end of the bar, the residual wave goes through the cylinder into the transmission bar. Strain gauges affixed to the incident and transmission bars measure the strains caused by the elastic wave pulse. To optimize the transmitted pulse, we incorporated a pulse shaping technique where a thin copper disk is affixed on the impact surface of the incident bar to shape the incident pulse [3]. The system set up is shown in Figure 10 and SOP is attached as Appendix B.

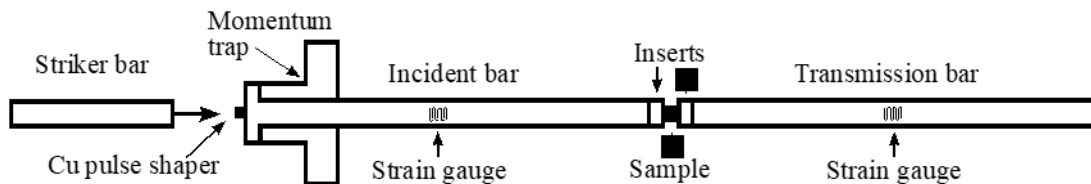


Figure 10. Split Hopkinson compression test

Three tests were conducted on H2/H15 and H15/Sn cylinders manufactured using the same process used to make the RM casings. Split Hopkinson bar test data already existed for pure H15. The first experiment was a moderate strain rate test. Cylinders with dimensions approximately 10mm x 10mm of H2/H15 and H15/Sn RMs were loaded in a bar setup as shown in Figure 10. A striker bar with density 8.278g/cc, length 304.8 mm and diameter 19.05 mm was used. Table 2 lists the mass and dimensions of the cylinders, and impact velocity of the striker bar.

Table 2. Moderate strain rate (19.05mm diameter striker bar)

Sample #	Mass(g)	Length(mm)	Diameter(mm)	Impact velocity (m/s)
H2/H15				
1	2.45	9.63	10.85	13.86
2	2.51	9.08	10.89	22.91
3	2.14	8.22	10.90	29.70
H15/Sn				
1	2.55	10.06	10.66	13.17
2	2.54	10.05	10.64	23.26
3	2.53	10.05	10.64	29.60

The moderate strain test is followed by a high strain test using similar set up but smaller bar. A striker bar with density 8.278g/cc, length 304.8 mm and diameter 9.525 mm is used in the high-strain experiment. The diameter and length of the samples here are approximately half those of the moderate strain experiments. The smaller diameter of the striker bar and specimen increase the strain rate considerably. This can be seen in Table 3 as the impact velocities are almost double that of the moderate strain test.

Table 3. High strain rate (9.525 mm diameter striker bar)

Sample #	Mass(g)	Length(mm)	Diameter(mm)	Impact velocity (m/s)
H2/H15				
1	0.34	5.18	5.70	24.80
2	0.33	5.11	5.58	40.36
3	0.32	5.02	5.57	51.79
H15/Sn				
1	0.34	5.06	5.50	24.95
2	0.33	5.02	5.46	40.21
3	0.33	5.02	4.47	52.60

Table 4. Dynamic Brazilian test samples

Sample #	Mass(g)	Length(mm)	Diameter(mm)	Impact velocity (m/s)
H2/H15				
1	1.20	5.07	10.73	14.44
2	1.21	5.09	10.83	14.02
3	1.17	5.10	10.74	13.88
H15/Sn				
1	1.30	5.07	10.87	14.18
2	1.27	4.94	10.83	14.13
3	1.31	5.08	10.83	13.94

The last experiment on the Split Hopkinson bar is a dynamic Brazilian test which is an indirect but very efficient way to determine the tensile strength of materials. The system configured shown in Figure 11 is similar to the moderate strain test with one major variation. The sample is wedged circumferentially in between the incident and transmission bars. Table 4 lists the data of the samples tested.

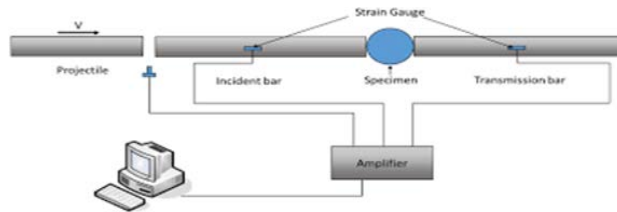


Figure 11. Split Hopkinson Dynamic Brazilian test set up

D. SOUND SPEED TEST

The propagation speed of longitudinal and transverse mechanical waves in H2/H15 and H15/Sn samples in Figure 12 were determined using ultrasound waves and the pulse-echo technique facilitated by an ultrasonic couplant. The ultrasound was generated by an Olympus Panametrics-NDT Pulser/Receiver Model 7072PR. A Tektronix DPO71254 oscilloscope was used to monitor the signals (Figure 13). Once the distinct echo pattern was seen, the time between reflections was measured using the oscilloscope. The speed of the wave calculated by dividing twice the sample thickness by the time between reflections.

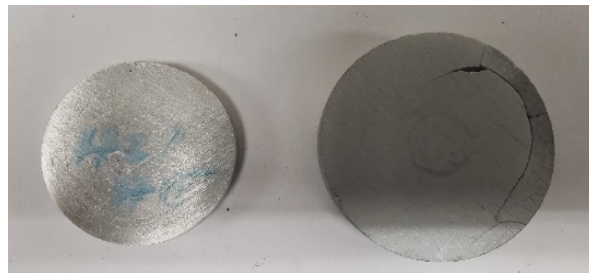


Figure 12. Sound speed test samples. H2/H15(left), H15/Sn (right)



Figure 13. Tektronix DPO 71254 Digital Phosphor Oscilloscope (left) and Olympus Model 5072PR Pulser/Receiver (right)

E. FRAGMENTATION ANALYSIS

H2/H15, pure H15 and H15/Sn RM samples were launched in a single-stage gas gun into aluminum plates to determine their ballistic impact and fragmentation properties. The metal fragments generated from impact are collected in an artificial snow medium and separated for analysis [4]. Figure 14 is a schematic of the single stage gas gun used and Table 5 has the data of the sample tested. The fragments are separated immediately to avoid oxidation using the filtration process developed by Booth-Seay that would quickly remove the artificial snow while retaining as much fragment mass as possible [5].

Table 5. Single stage gas gun sample data

Sample #	Mass(g)	Length(mm)	Diameter(mm)	Shot velocity(m/s)
H15				
1	2.05	9.97	9.98	517
2	2.04	9.98	9.96	627
3	2.06	10.00	9.97	565
H2/H15				
1	1.99	9.99	9.97	886
2	2.03	9.98	9.95	563
H15/Sn				
1	2.30	10.02	9.97	550
2	2.25	10.00	9.98	518
3	2.00	10.03	9.98	620

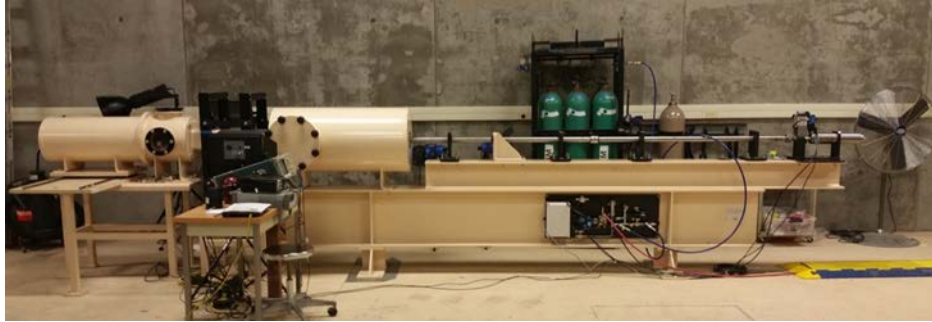
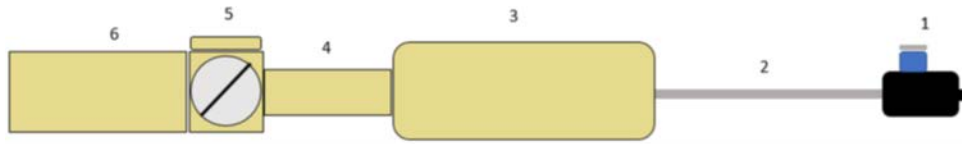


Figure 14. Schematic and image of the 0.5” Single Stage Gas Gun

F. EXPLOSIVE LAUNCH EXPERIMENT

The high strain rate fragmentation behavior of H15 aluminum was evaluated by detonating aluminum cold isostatically pressed cases filled with explosive. Detonation experiments were performed in the Hazardous Ordnance and Gunfire (HOG) chamber at Rocky Mountain Scientific Laboratory in Denver, Colorado. The chamber was approximately 1m in diameter and 1m in length. Sensitized nitromethane was used as the liquid explosive. The sensitized nitromethane was prepared by mixing 95% nitromethane with 5% ethylenediamine. This mixture is commonly known as Picatinny liquid explosive (PLX). Endcaps for the cases were machined from 6061 aluminum alloy and attached to the H15 case using RTV silicone sealant. Table 6 has data of the samples tested and the high explosive (HE) and detonator used. Figures 15 and 16 are the images of the cases and Figure 17 shows a complete charge assembly consisting of Al H15 case, 6061 Al endcaps, PLX explosive fill, and RP 80 detonator.

Table 6. HOG detonation sample data

Shot #	Material	M/C	Mass (g)	Bottom / Top endcap mass(g)	Detonator
1	H15	~2	81.3	7.3 / 7.5	RP-80
2	H15	~2	82.2	7.6 / 7.9	RP-80
3	H15	~3	126.4	7.8 / 7.2	RP-80
4	H15	~3	126.7	9.6 / 7.45	RP-80
5	Al 6061	~2	85.7	8.3 / 8.2	RP-80
6	Al 6061	~3	139	9.26 / 8.1	RP-80



Figure 15. CIPed H15 Al cases M/C 2 (top) and M/C 3 (bottom).



Figure 16. Al 6061 M/C 2 (top) and M/C 3 (bottom).

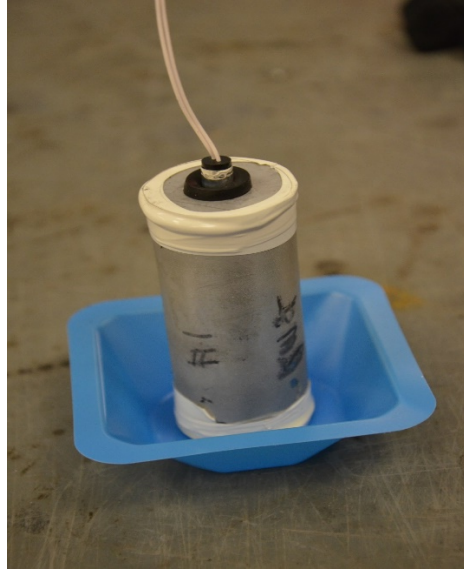


Figure 17. Charge assembly consisting of Al H15 case, 6061 Al endcaps, PLX explosive fill, and RP 80 detonator.

The fragments from the detonations were caught in freshly shaved ice to prevent secondary fragmentation on the HOG walls. Figure 18 shows the HOG chamber filled with snow before each shot, the density of the snow was approximately 0.3 g/cc. A 15.2 cm by 20.3 cm cavity was created around the charge, as shown in Figure 19.

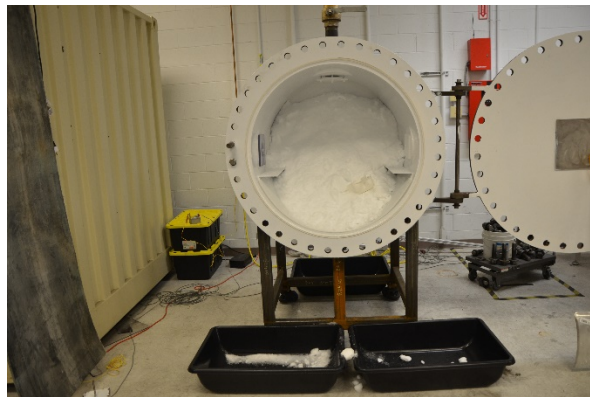


Figure 18. Snow filled HOG chamber for soft catch



Figure 19. Charge assembly hanging in snow cavity

Following each detonation, the snow was removed from the chamber and melted by addition of warm ethanol. The fragments were recovered in ethanol and washed with acetone then dried. The sizes of the fragments were characterized using the optical particle sizer used to analyze the fragments from the light gas gun.

III. RESULTS AND DISCUSSION

A. MECHANICAL PROPERTIES

1. Density and Porosity

The samples used during this experiment are manufactured in the NPS shock physics laboratory as described in section II. Table 7 shows the density and M/C ratio of the cases to be tested at RMSL. The average densities of the three variations of Al RM tested were determined using the simple mass/volume method in Equation 1. Table 8 illustrates the average densities and porosities of H2/H15 and H15

$$\rho = \frac{m}{v}, \quad (1)$$

where ρ is density, m is mass and v is the volume of the sample.

Table 7. Density and M/C ratio of CIPed cases

Sample #	Mass(g)	Volume(cc)	Density(g/cc)	M/C ratio
1	78.60	31.76	2.47	1.79
2	82.00	33.26	2.47	1.86
3	79.00	32.43	2.44	1.79
4	81.30	35.21	2.31	1.85
5	82.20	33.24	2.47	1.87
6	84.10	35.80	2.35	1.91
7	85.50	36.21	2.36	1.94
8	126.00	52.34	2.41	2.87
9	122.00	48.47	2.52	2.77

The average densities were then compared to the density of aluminum 6061-T6 to determine the porosity of the CIPed RMs using Equation 2

$$\frac{\rho(T6) - \rho(SRM)}{\rho(T6)} \times 100\% , \quad (2)$$

where $\rho(T6)$ and $\rho(SRM)$ are the densities of the T6 and Al RMs, respectively.

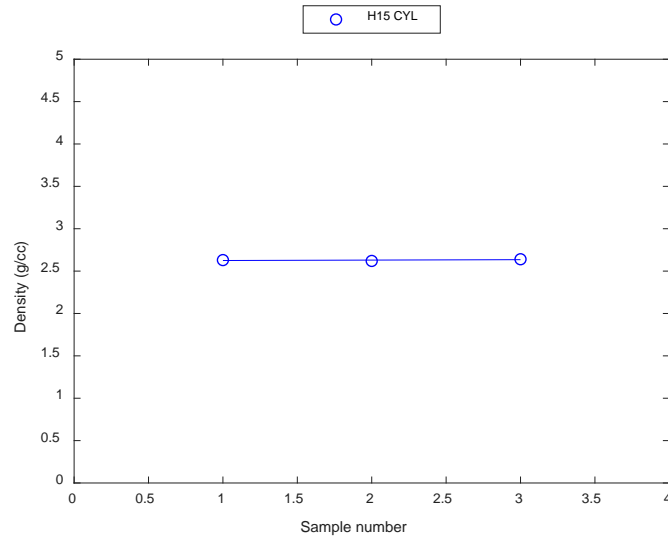


Figure 20. Density variations of H15 cylinders used in experiment

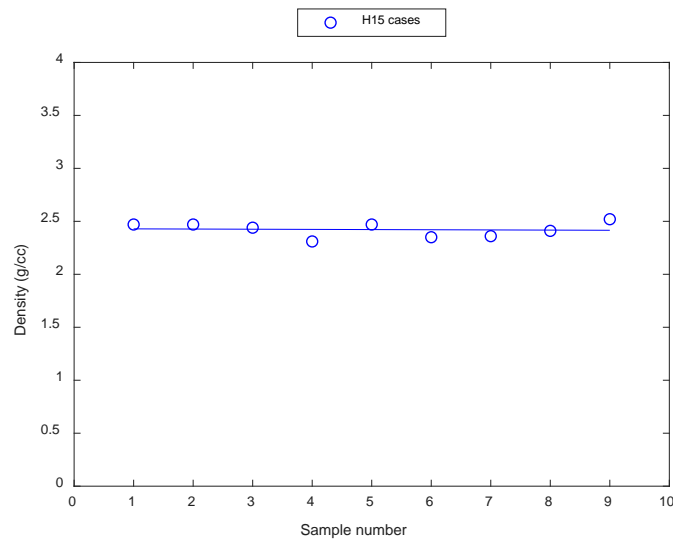


Figure 21. Density variations H15 cases used in experiment

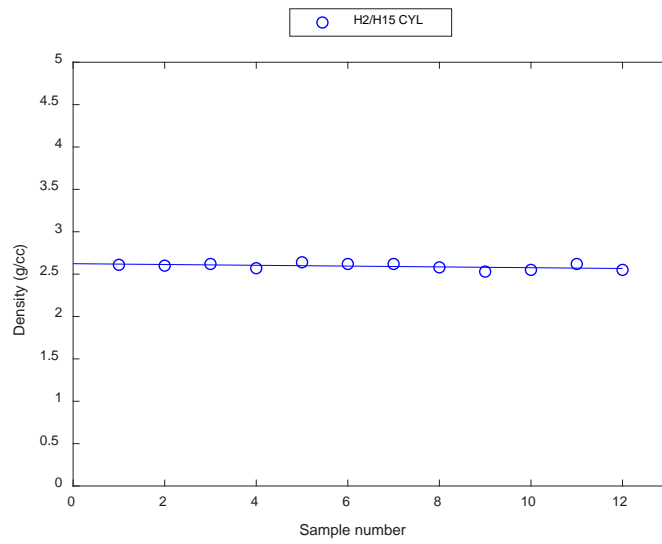


Figure 22. Density variations of H2/H15 cylinders used in experiment

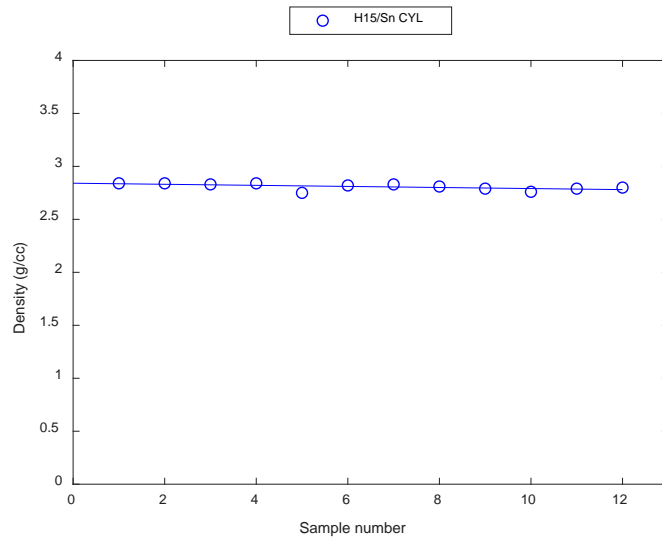


Figure 23. Density variations H15/Sn cylinders used in experiment

Figures 20 through 23 show the density spread of the samples used in this experiment. As illustrated in Table 8, the RM CIPing process described in Chapter II produced RM cylinders that are between 95% to 97% of TMD and cases at 90% TMD. The average

density of the H15 cylinder was 1.5% higher than H2/H15 mixture, indicating that the bimodal powder mixture does not aid significantly in improving post-CIP densities.

Table 8. Average densities and porosities of Al RMs

	Al 6061 (T6)	H15 (CYL)	H15 (Cases)	H2/H15 (CYL)	H15/Sn (CYL)
Average density(g/cc)	2.7	2.63	2.42	2.59	2.81
Average porosity (%)	0	2.6	10.4	4.1	2.1

Also of note is the significant differences between the average densities and porosities of H15 cylinders and cases. This may be due in part to the hydrostatic pressure on the powder in the CYL mold being distributed evenly, while the powder in case mold were constrained at the ends by the mandrel as shown in figure 24. Secondly, the density of the H15/Sn mixture is 4.4% higher than the density of T6. This increase in density is solely because the density of Sn (7.31g/cc) is much higher than T6 and adding 10% wt increased the overall density by 4.4%. The addition of tin does reduce the porosity to small levels, but as discussed below this does not result in a significant improvement in tensile strength.

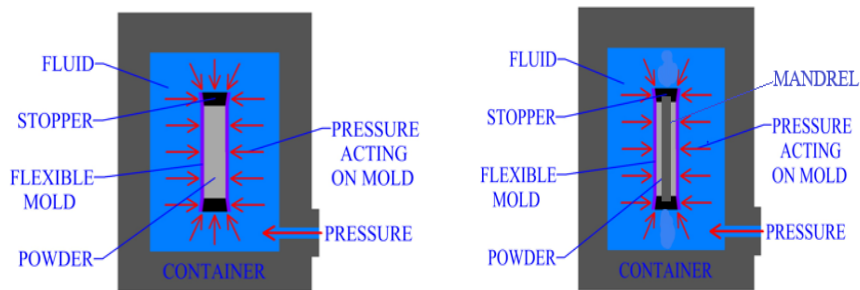


Figure 24. CIP hydrostatic pressure distribution on cylinder (left) and case (right).

2. Longitudinal and Shear Sound Speed

Sound waves in metals are made up of longitudinal waves and shear wave. Shear waves occur in solids and travel at a slower speed. The longitudinal sound speed is determined by the materials compressibility, shear modulus and density. The shear sound speed is only determined by the shear modulus and density. The longitudinal sound speed, c_l and the shear sound speed, c_s are calculated using equations (3) and (4), respectively,

$$C_l = \frac{2t}{T} \quad (3)$$

$$C_s = \frac{2t}{T} \quad (4)$$

where t is the thickness of the sample used and T is the time elapsed for one complete cycle which is twice the thickness.

Table 9. H15/Sn sound speed test data ($t = 7.4\text{mm}$)

Longitudinal sound speed, c_l		
Range (μs)	Time, $T(\mu\text{s})$	Sound speed, $c(\text{m/s})$
4.76 – 2.42	2.34	5555.6
4.65 – 2.53	2.12	6132
6.67 – 4.63	2.04	6372.6
6.76 – 4.78	1.89	6878.4
Shear sound speed, c_s		
Range (μs)	Time, $T(\mu\text{s})$	Sound speed, $c(\text{m/s})$
7.12 – 2.84	4.28	3037.4
11.38 – 7.12	4.26	3051.6
15.64 – 11.38	4.26	3051.6
28.84 – 24.56	4.28	3037.4

Table 10. H2/H15 sound speed test data (t = 6.5mm)

Longitudinal sound speed		
Range (μs)	Time, T(μs)	Sound speed, c(m/s)
5.57 – 2.78	2.79	5304.6
8.17 – 5.57	2.6	5692.2
5.71 – 3.12	2.59	5714.2
8.28 – 5.70	2.58	5736.4
Shear sound speed		
Range (μs)	Time(μs)	Sound speed, c(m/s)
8.82 – 3.72	5.1	2902
13.94 – 8.82	5.12	2890.6
19.02 – 13.94	5.08	2914
34.88 – 29.76	5.12	2890.6

3. Moduli

Figures 25 through 31 show stress/strain data from Split Hopkinson pressure bar testing. The plots compare the ultimate yield and tensile strength of the three variations of Al RMs at different strain rates ranging from 600s^{-1} to 3500s^{-1} . H15 and H2/H15 have similar yield strengths of about 140MPa at 600s^{-1} strain rate and all three RMs have yield strengths around 160MPa at 1200s^{-1} strain rate.

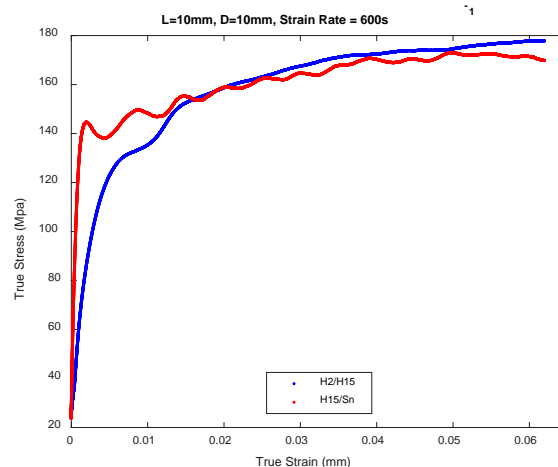


Figure 25. Stress/strain plot H2/H15 and H15/Sn (moderate strain rate)

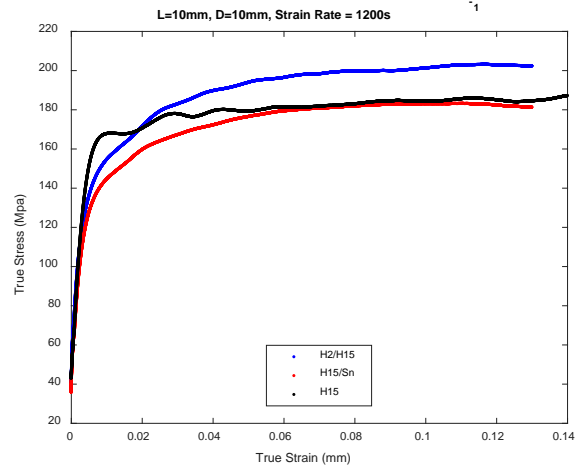


Figure 26. Stress/strain plot H2/H15, H15/Sn and H15 (moderate strain rate)

Figure 26 suggests that the H2/H15 has a slightly higher strength compared to H15 and H15/Sn at intermediate strain rates. All MATLAB codes for Split Hopkinson Pressure bar test is attached as Appendix C.

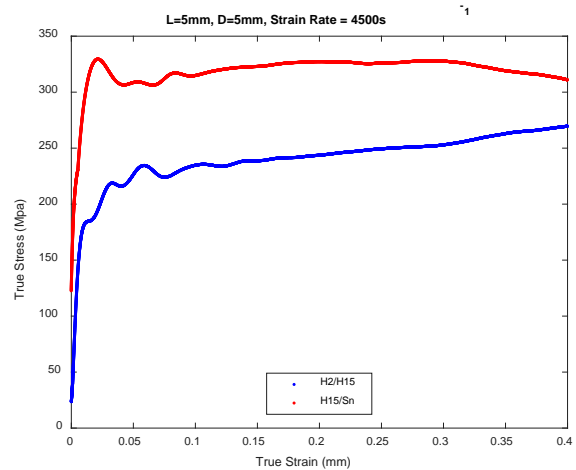


Figure 27. Stress/strain plot H2/H15 and H15/Sn (high strain rate)

Figure 27 shows that H15/Sn has a significantly higher strength as the strain-rate increases.

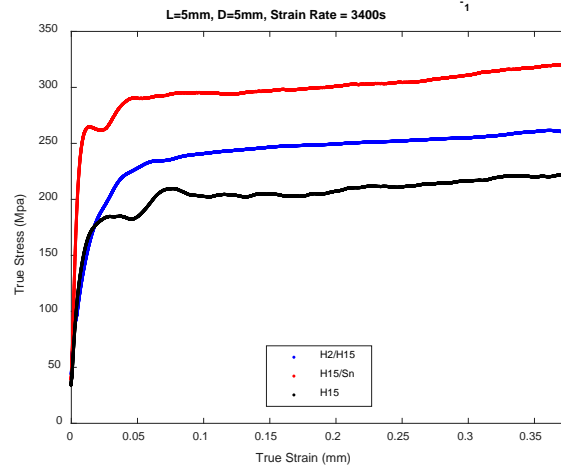


Figure 28. Stress/strain plot H2/H15, H15/Sn and H15 (high strain rate)

Figure 28 shows H15/Sn shows some evidence of rate-hardening, as the yield point increases significantly more than the pure aluminum compounds as the strain rate increases. This is worth further investigation in the future.

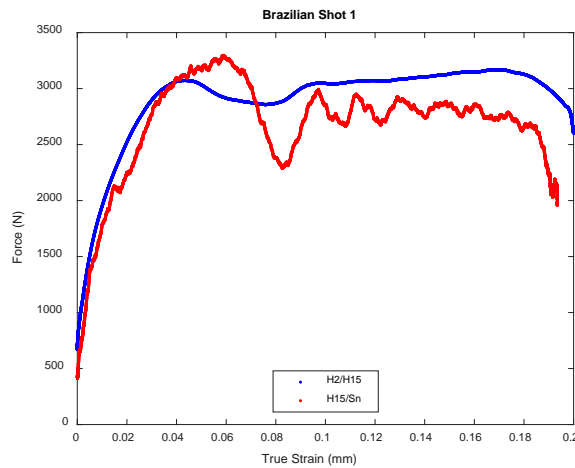


Figure 29. Dynamic Brazilian test 1, H2/H15 and H15/Sn

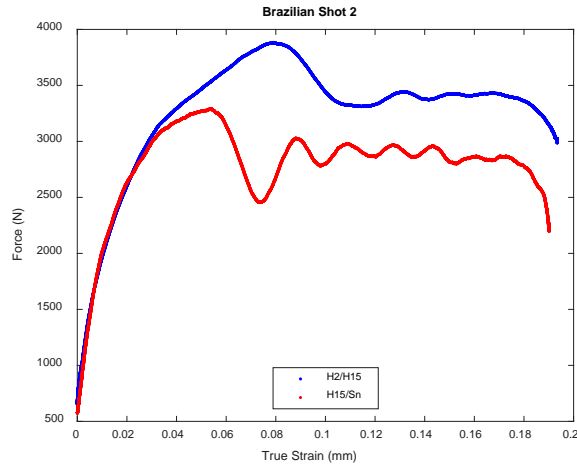


Figure 30. Dynamic Brazilian test 2, H2/H15 and H15/Sn

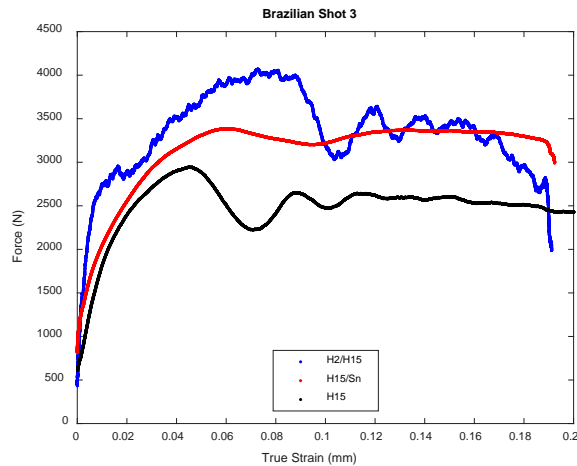


Figure 31. Dynamic Brazilian test 3, H2/H15, H15/Sn and H15

The tensile strengths in Table 11 were calculated using data from the dynamic Brazilian test which is an indirect method to determine the tensile strength of brittle materials. The tensile strength is calculated assuming that failure will occur at the center of sample at the point of maximum tensile stress [6] as illustrated in the frame captures and DIC E_{yy} images in Figures 32 and 33. Equation (5) is used to calculating the tensile strength [6]

$$\sigma_t = \frac{2P}{\pi Dt}, \quad (5)$$

where P is the peak load (N), D is the diameter of the sample (mm), and t is the thickness of the sample measured at the center (mm). The peak force P is taken directly from the strain-gauges on the Hopkinson bar, shown in raw form in Figures 29-31.

The P-wave modulus, M and the shear modulus, G are calculated using equations (6) and (7)

$$M = \rho c_l^2 \quad (6)$$

$$G = \rho c_s^2, \quad (7)$$

where ρ is density of the specimen, c_l is the longitudinal sound speed, and c_s is the shear sound speed.

Table 11. Mechanical properties of Al RMs compared to Al 6061

	T6	H15	H2/H15	H15/Sn
Longitudinal sound speed, c_l (m/s)	6420	5074	6234.65	5611.85
Shear sound speed, c_s (m/s)	3040	2775	3044.5	2899.3
P-wave modulus, M (GPa)	111.3	67.7	101	88.5
Shear modulus, G (GPa)	26	20	24	23.6
Elastic modulus, E (GPa)	68.9	52.1	64.5	62.2
Bulk modulus, K (GPa)	67.5	40.7	68.7	57
Poisson ratio, ν	0.33	0.29	0.34	0.32
Tensile strength (MPa)	276	35	47.2	37.2

The two moduli calculated above are then used to determine the elastic modulus (E), bulk modulus (K), and Poisson ratio (ν) for the three Al RMs using the Lamé constant [7] conversion formula in equations (8) through (10).

$$E = \frac{(3M-4G)}{M-G} \quad (8)$$

$$K = M - \frac{4G}{3} \quad (9)$$

$$\nu = \frac{(M-2G)}{(2M-2G)} \quad (10)$$

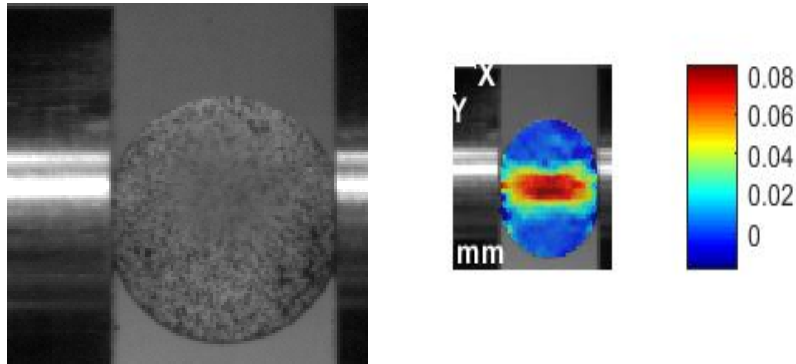


Figure 32. Frame captured from H15 Dynamic Brazilian test (left), DIC E_{yy} strain image (right) just before the tensile crack opens.

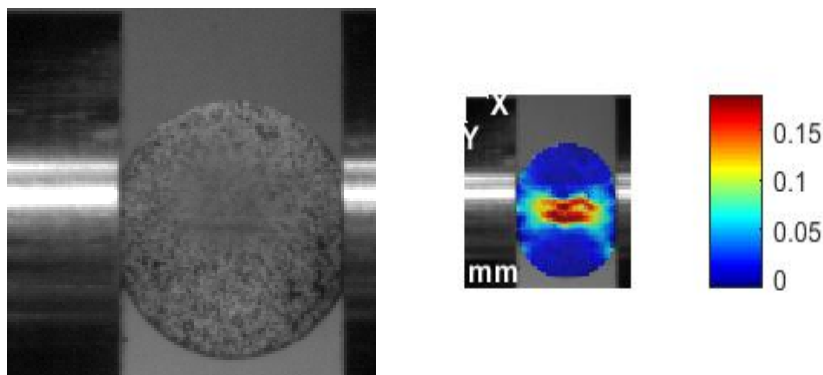


Figure 33. Frame captured from H15 Dynamic Brazilian test (left), DIC E_{yy} strain image (right) just after the tensile crack opens.

B. FRAGMENTATION ANALYSIS

Projectiles of all three materials were fired into perforation plates and the debris was recovered in a soft-catch medium of artificial snow. Debris was analyzed with an optical camsize to measure the fragment distribution. Data is presented below as the mass probability density function (PDF) and mass cumulative distribution function (CDF), similar to previous NPS RM analysis such as that done by Booth-Seay [5]. The experimental data is then fit to determine characteristic size parameters. All data was successfully fit by the bimodal mass PDF equation

$$m(s) = \chi\beta \exp(-\beta(s - s_0)) + (1 - \chi) \frac{1}{6\mu} \left(\frac{s}{\mu}\right)^3 \exp\left(-\frac{s}{\mu}\right). \quad (11)$$

Here, the two modes are a power-law form for the very small fragments (the first term), and a traditional Mott-type distribution for the larger fragments. Similar forms have previously been used to fit fragmentation for aluminum RMs [4]. In this equation m is the PDF over the fragment size s , β is a fit parameter for the power-law mode (potentially related to the extent to which fast-running cracks microbranching), μ is related to the characteristic fragment size of the Mott-type mode, χ is a weighting parameter that sets how much of each mode is present, and s_0 is a lower-bound on fragment size and is set to a constant $44\mu\text{m}$.

The results of these fits are shown in Table 12 and Figures 34 through 36 (MATLAB codes attached in Appendix C). With one exception, the trends in the data are as expected; as impact velocity into the plate increases, the portion of fine fragments (governed by χ) increases, and the characteristic fragment size of the larger mode μ goes down. The exception to this is the pure H15 material, where the lower velocity 565 m/s shot has smaller fragments than the shot at 627 m/s. This should be repeated in future work, and is very likely a consequence of a large void or dominant defect present in the particular sample that was fired. Extensive analysis of the fragment patterns and interpretation can be found in prior NPS theses and articles [4], [5]. Here the primary result is shown in Figure 37 (MATLAB code attached in Appendix C), which compares each of the three tested materials at a comparable impact velocity. The overall fragment distribution for each of

these three materials differs slightly but overall is very similar. In other words, the addition of tin of a bimodal mixture of aluminum powders does not drastically alter the fragment pattern produced when a reactive fragment perforates a thin plate. Figures 38 through 40 are images of the fragments for each type of RM tested.

Table 12. Fragment distribution fit parameters

Material	Velocity (m/s)	χ	β (1/mm)	μ (mm)
H15	627	0.43	0.25	1.46
H15	565	0.44	0.91	1.02
H2/H15	886	0.48	2.0	0.586
H2/H15	563	0.89	0.40	10
H15/Sn	620	0.47	1.2	0.76
H15/Sn	550	0.47	1.02	1.15
H15/Sn	518	0.50	0.25	2.74

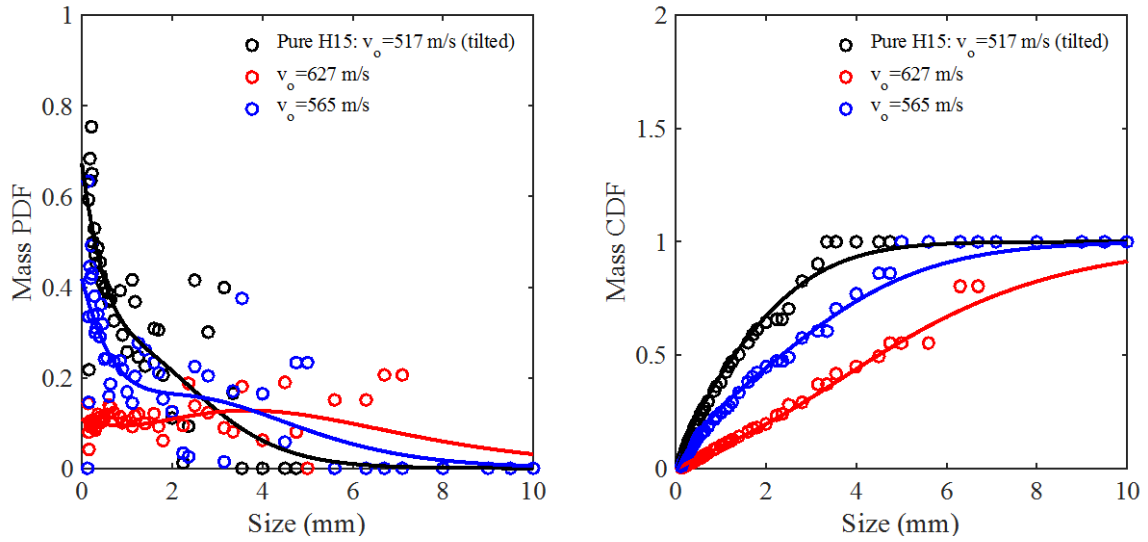


Figure 34. Fragment distributions from pure H15 projectiles. Note that the data shown in black is for a projectile that tilted prior to impact.

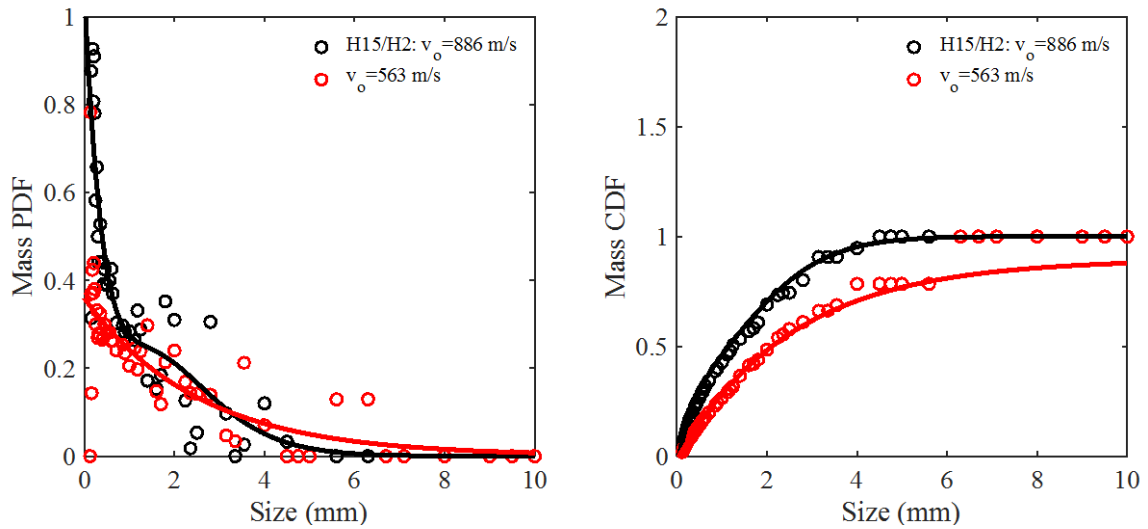


Figure 35. Fragment distributions from projectiles made from an H15/H2 mixture.

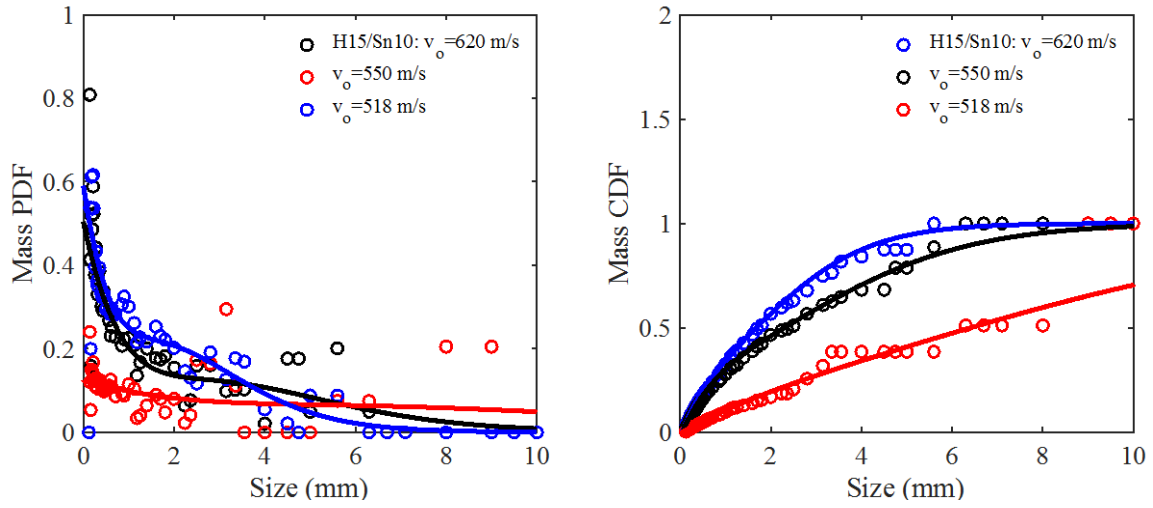


Figure 36. Fragment distributions for the H15/Sn10 projectiles.

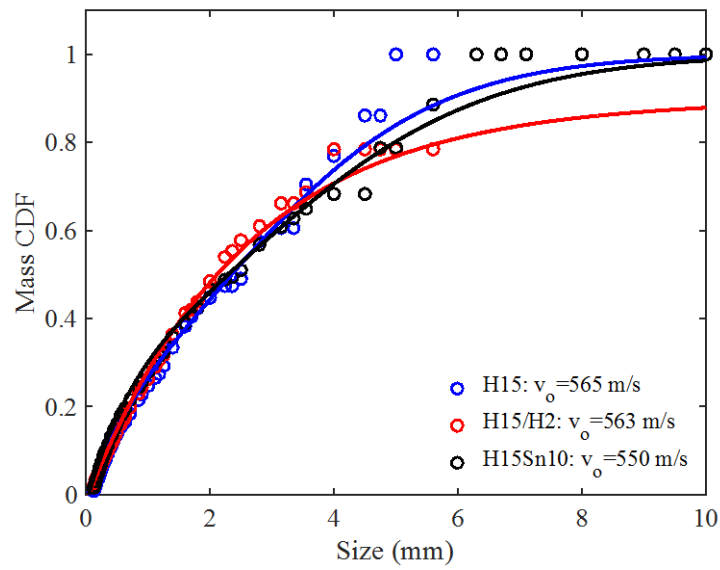


Figure 37. Cumulative distribution functions of all three materials at comparable velocities, showing similarities in the characteristic particle size.



Figure 38. H15 light gas gun fragments at 565 m/s



Figure 39. H2/H15 light gas gun fragments at 563 m/s



Figure 40. H15/Sn light gas gun fragments at 550 m/s

C. EXPLOSIVE LAUNCH

Initial mass probability density function (PDF) and mass cumulative distribution function (CDF) analysis for the fragments collected at RMSL is shown in Figure 41. More than 60 percent of the fragments from H15 cases were under 1mm and up to 80 percent under 2mm. Compared to less than 10 percent and 20 percent respectively for T6. Figure 42 shows images of the fragments after separation.

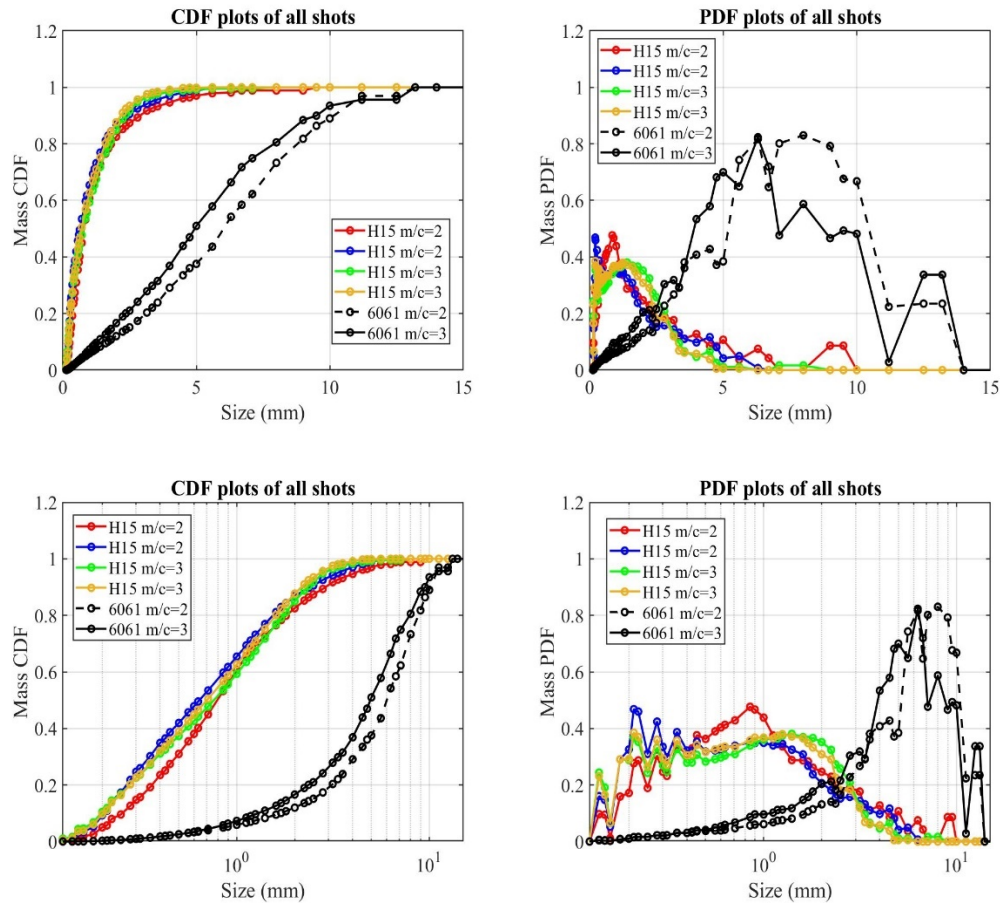


Figure 41. CDF and PDF of H15 and T6 cases from explosive launch experiments at RMSL

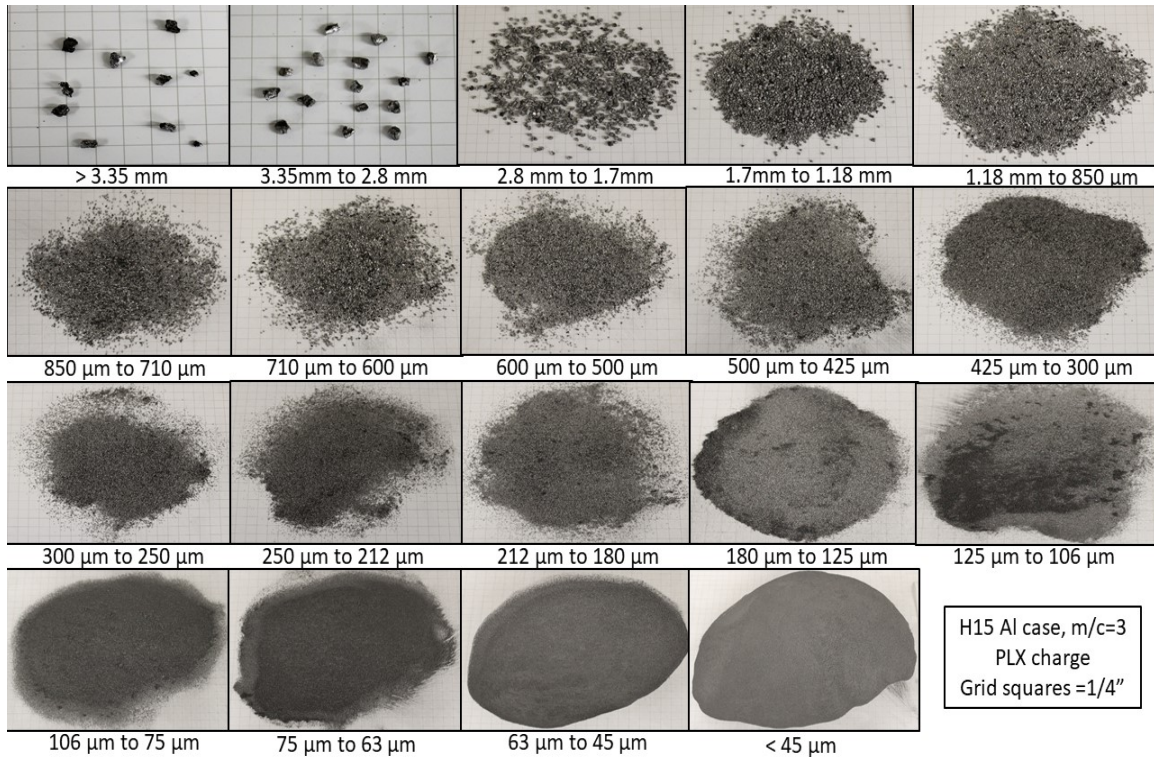


Figure 42. Images of all the fragments sieved out by particle size

IV. CONCLUSION AND FUTURE WORK

The mechanical properties of the H2/H15 mixture are generally found to be only marginally better than those of the H15. The addition of tin increased the density of the sample and lowered the porosity by almost 20%. The Sn variation also showed evidence of a higher degree of rate hardening at high strain-rates. H15 is found to have slightly less porosity than H2/H15, but this did not translate into better yield and tensile strength. H2/H15 surprisingly had slightly better tensile strength in the dynamic Brazilian test even with a higher porosity. Overall, pure H15 was easily CIPed and machined, making it the best option out of the three to make the initial cases for explosive charge test. The fragment collection from the explosive tests looks as expected, and future work will focus on a detailed analysis of these fragments as compared to gas gun impact results.

THIS PAGE INTENTIONALLY LEFT BLANK

APPENDIX A. COLD ISOSTATIC PRESS STANDARD OPERATING PROCEDURE

A. REQUIRED MATERIALS AND EQUIPMENT



Figure 1. Powder preparation required material

Figure 1 illustrates the required material for powder preparation.

- Muffle Furnace
- Balance
- Ball Mill
- Zinc Dust Powder
- Stainless Steel 304 Powder
- Ethanol
- Swabs
- Weighing Paper
- 2 Ceramic boats
- Mill Jar
- Styrofoam
- CIP Mold(s)
- Gloves
- 3 Spatulas
- Duct Tape
- Kimtech Wipe
- Wypall Cloth
- Razor

B. POWDER PREPARATION

1. Place Wypall cloth on over working surface. Be sure to perform all work with loose powders over this cloth with gloves.
2. Use a spatula to put the metal powder in a ceramic boat for each metal. Ensure the powders stay separate using 2 ceramic boats and 2 spatulas to avoid cross contamination.
3. Place both ceramic boats in the muffle furnace, Figure 2 and set the temperature to 60°C for about 30 minutes. This process is used to dry out the metal powders.



Figure 2. Muffle furnace.

4. After removing the powders from the muffle furnace, weigh the appropriate amount of powder on the balance using weighing paper, Figure 3.

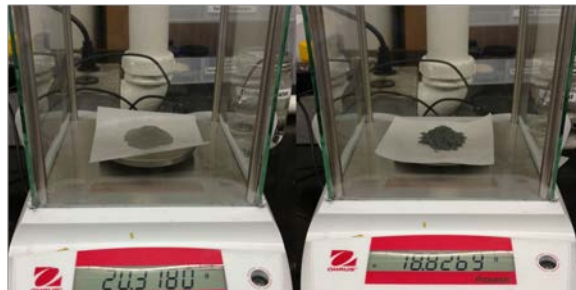


Figure 3. Micro balance.

5. Place both metal powders in the mill jar, Figure 4. Tightly secure the lid of the mill jar.



Figure 4. Mill jar.

6. Secure the mill jar in the Ball Mill by tightening the screw illustrated in Figure 5.



Figure 5. Mill jar secured in a ball mill.

7. Close the lid of the ball mill, Figure 6. Turn the power on using the toggle switch in the lower back right corner of the machine. Set the timer on the front of the machine for 30 seconds. Push START.



Figure 6. Ball mill machine

8. Once the timer reaches 0, the ball mill machine will stop shaking. Turn off the power to the machine using the same toggle switch on the lower back right corner. Open the lid and remove the mill jar.
9. Open the lid of the mill jar. Using the clean spatula, carefully transfer the mixed powder to the desired CIP mold, Figure 7.



Figure 7. Filling CIP mold

10. Periodically tap the mold to help settle the powder to ensure gaps are filled. Fill them old until there is just enough room for the mold top to fit, Figure 8. If required, fill excess space with Styrofoam. Overfilling the mold may cause the top to not seal and the sample to crack in the pressing process.



Figure 8. Full CIP mold

11. Wipe clean the top lip of the CIP mold using swabs and kimtech wipes. It may be necessary to use some ethanol. The seal between the mold and top is important.
12. Using strips of duct tape, secure the mold top. Best technique is to place two strips on the top in a cross down the length of the mold, then wrap additional strips spiraling down the mold; as illustrated in Figure 9.



Figure 9. Mold taping technique

13. The sample is ready to be pressed in the CIP. The unused, uncontaminated powder may be returned to its respective container. Clean the ceramic boats, spatulas and mill jar with ethanol using kimtech wipes and swabs as necessary.

C. PARTS OF THE COLD ISOSTATIC PRESS

Figures 10 and 11 illustrate the parts of the Cold Isostatic Press (CIP) with a front and top view, respectively.



Figure 10. Front view of CIP

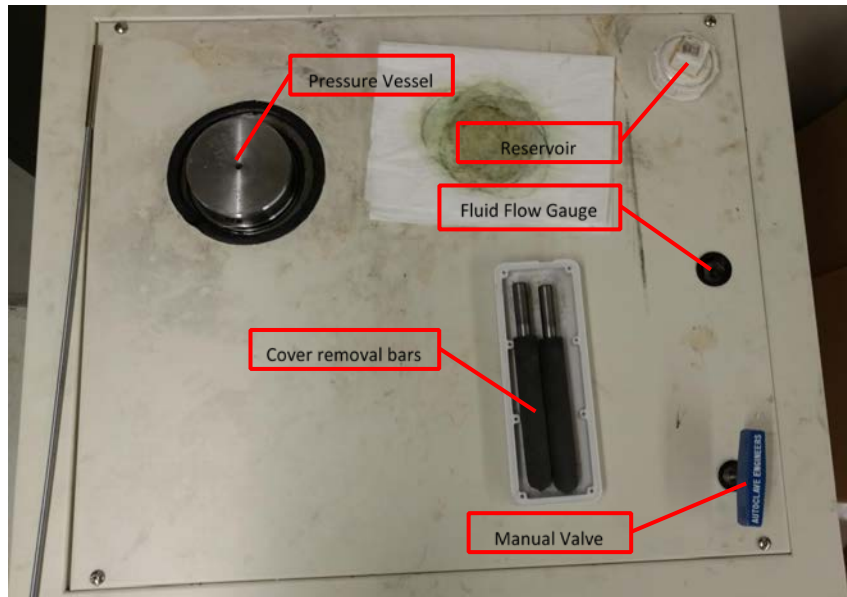


Figure 11. Top view of CIP

D. PRESSING PROCEDURE

1. Ensure the power is off by depressing the STOP button and the power indicator is not illuminated, Figure 12. Check to make sure the CIP is unplugged.



Figure 12. Power indicators

2. Set the desired pressure on the pressure gauge using the black knob on the front to move the contact arm to the desired pressure, Figure 13.

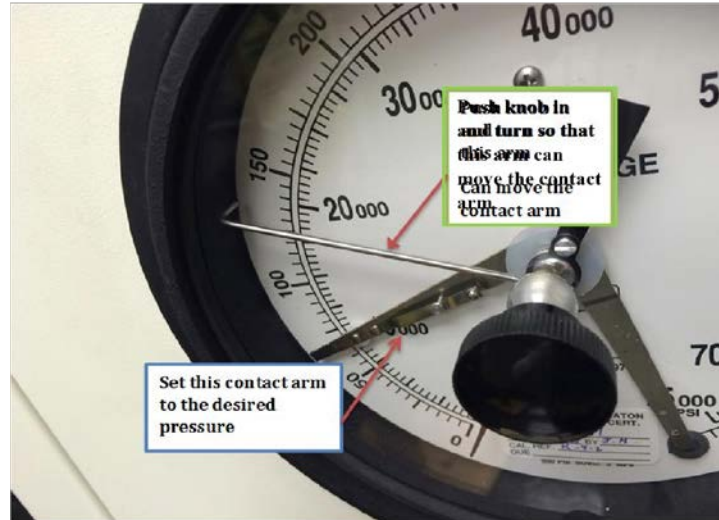


Figure 13. Pressure gage setting

CAUTION: Do not adjust the contact arm with electrical power on, there is an electrical current running through the arm.

WARNING: Do not set pressure above 60,000psi.

3. Ensure the manual valve is open to allow any residual pressure to vent.
4. Place the cover removal bars in the holes of the pressure vessel top cover, Figure 14. Turn counterclockwise to remove the cover. Check the o ring at the base of the top cover for any nicks or tears.



Figure 14. Cover removal bar in top cover



Figure 15. Place sample in pressure vessel

5. Place the item to be pressed in the pressure vessel, Figure 15.
6. Check the fluid level in the pressure vessel. The fluid should be 1.5 to 2 inches below the bottom thread, Figure 16. Excess fluid can be removed from the pressure vessel and poured into the reservoir.

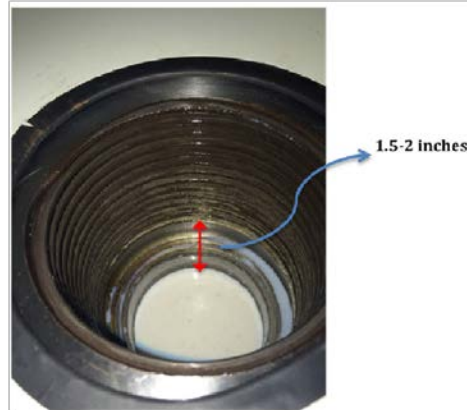


Figure 16. Fluid level inside pressure vessel

7. Replace the pressure vessel top cover. Once tightened, loosen the cover a quarter of a turn to make cover removal easier. NOTE: The tightness of the cover does not affect the seal.
8. Check to make sure the fluid level in the reservoir is below the return line, Figure 17.

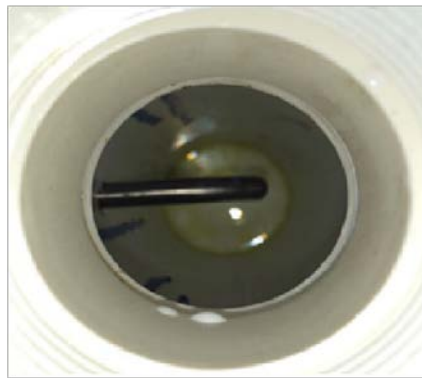


Figure 17. Return line in reservoir

CAUTION: The pneumatic pump is loud, ensure you are wearing hearing protection prior to starting the pump.

9. Plug the power cord into the wall outlet. Turn the power on by pulling out the STOP button. Ensure the power indicator is illuminated, Figure 18.



Figure 18. Pull out STOP button to provide power to the CIP

10. Start the pump by toggling the pump power switch to ON. The toggle switch should illuminate, Figure 19.

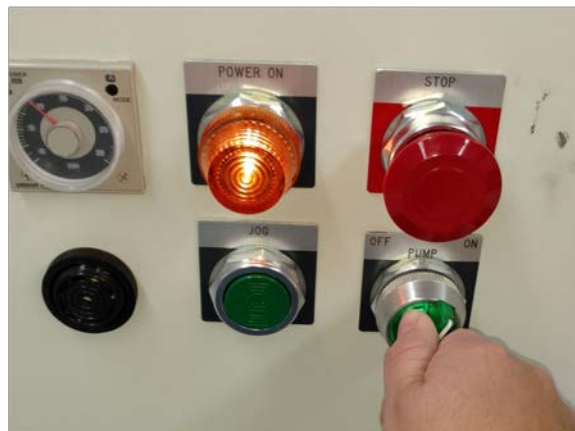


Figure 19. Pump power toggle switch

11. Watch the fluid flow gauge. Once there is a constant fluid flow from the pressure vessel to the reservoir, close the manual valve by turning it clockwise. Do not overtighten the valve but ensure the fluid stops flowing once closed.
NOTE: The pump can be stopped at any time by toggling the pump power switch to OFF and pushing the STOP button.

12. Once the pressure gauge makes contact with the contact arm, the pump will automatically stop. Start a stop watch for desired dwell time.
NOTE: If the pump stops before reaching desired pressure and making contact with the contact arm, depress the JOG push button. JOG will not work once the pressure arm makes contact with the contact arm.
13. After desired dwell time, toggle the pump power switch to OFF.
14. Slowly depressurize the pressure vessel by opening the manual valve while monitoring the pressure gauge. If pressure is released too rapidly, it is possible for the sample to break apart.
15. Once all the pressure is released and the manual valve is completely open, shut power by pushing the STOP button.
16. As before, open the pressure vessel top cover and remove the sample. Sample removal may be tricky, oftentimes the metal grabber is sufficient to grab the mold, Figure 20. However, it may be necessary to reach in the pressure vessel with your arm.



Figure 20. Remove sample from pressure vessel

17. Repeat process for desired number of samples. Once complete, screw top cover back into place and unplug the CIP.

APPENDIX B. SPLIT HOPKINSON PRESSURE BAR STANDARD OPERATING PROCEDURE

1. Set incident bar
 - I. Slide the bar so that there is roughly 1" of space between the end of the launcher barrel and the front of the incident bar.
 - II. Engage momentum trap making sure the incident bar endcap, bar sleeve, and momentum trap are all in good mechanical contact.
 - III. Make sure the incident bar strain gauge wire isn't twisted up around the bar.
2. Load sample
 - I. Add a little grease to the bar faces.
 - II. If shooting something potentially dangerous to the bar faces, install bar inserts by adding a dab of high vacuum grease to hold the insert in place, then wrapping Teflon tape around the joint. Make sure there is good mechanical contact between the bars and the inserts.
 - III. Slide transmission bar over to clamp the sample in place, making sure that the transmission strain gauge wire doesn't get twisted around the bar.
3. Turn on and setup Phantom camera.
 - I. Plug in power to the camera.
 - II. Turn on phantom laptop
 - III. Open PCC 2.8 software.
 - IV. Adjust camera settings with lights on.
 - V. Turn lights off when not in use or they'll heat things up.
 - VI. Turn on the BNC delay generator box
4. Add pulse shaper to incident bar
5. Open up PicoScope software – Set trigger to none
6. Check strain gauges
 - I. Power on to amplifiers (red button on the bottom).
 - II. Current on to the strain gauges (silver switch labelled excitation).
 - III. Press down and hold for 1 sec both the auto-balance switches.
 - IV. Make sure they auto-balance correctly.
 - V. Check calibration by switching UP both Cal A switches, the reading should jump up to +2 Volts.
 - VI. If the gauges do not auto-balance or calibrate correctly, a strain gauge has likely popped, and needs replaced.
 - VII. Turn off current to the strain gauges (excitation again).
7. Charge gun to desired pressure
8. Once it's done charging (little beeps) use the tape measure to push the striker bar all the way back (should go in 24").

9. Pull the tape out then hit reset on the SureSpeed speedometer read out.

10. FIRING PROCEDURE

- I. Turn on current to strain gauges (excitation switch)
- II. Auto-balance and recheck calibrations
- III. Set picoscope software trigger to “single”.
- IV. Press “stop” on pulse generator box, then press “run”.
- V. Click capture in the phantom camera software
- VI. Fine trim strain gauges to make sure the lights are both off as much as possible.
- VII. Make sure SureSpeed speedometer reads “ready”
- VIII. Hold “arm” button the push fire.
- IX. Record velocity of striker ASAP, that number is critical and can vanish.
- X. Turn off current to strain gauges
- XI. Turn off camera lights
- XII. Save picoscope data as picoscope data file and as .txt.
- XIII. Save Phantom video.
- XIV. Repeat firing procedure as needed.

APPENDIX C. MATLAB CODE

A. PACKING EFFICIENCY PLOT MATLAB CODE

```
%% Packing Efficiency Plot

% Valimet Spherical Nominal Aluminum 50% Powder Specs
H2 = 3.5; H3 = 4.5; H5 = 8.0; H10 = 12.0; H15 = 20.0;
H30 = 31.0; H50 = 55.0; H60 = 70.0; H95 = 108;
D_fine = H2; % Fine diameter; for our purposes H2 ONLY
D_coarse = [H3,H5,H10,H15,H30,H50,H60,H95];
D_coarse_name = [3,5,10,15,30,50,60,95]';
D_10 = 10; % 10 microns diamter; desired
%%
% Packing Efficiency Mixtures Algorithm
PE_max=[];
PE_C = 0.6; % Pure assumption; may not be the best method
PE_F = 0.6; % Pure assumption; may not be the best method
Xf = 0.01:0.01:1.0; % Volume fraction
e = exp(1);
for j = 1:length(D_coarse)
    R = D_coarse(j) / D_fine;
    F1 = abs(( e .* Xf .* log( Xf )) .^ (1.25 ./ PE_C )); % Volume
    Fraction of Fine particles
    F2 = exp( -4 ./ R ); %
    Size ratio of coarse to fine particles
    PE_mix = PE_C + ( 1 - PE_C ) .* PE_F .* F1 .* F2;
    hold on
    plot(Xf,PE_mix)
    PE_max = [PE_max max(PE_mix)];
    vector = [Xf;PE_mix]';
    [PE_mix,index] = max(abs(PE_mix));
    Xf_max = Xf(index);
    Xf_10(j) = (D_10 - D_coarse(j)) ./ (H2 - D_coarse(j));
    F3(j) = abs(( e .* Xf_10(j) .* log( Xf_10(j) )) .^ (1.25 ./ PE_C
)); % Volume Fraction of Fine particles
    F4(j) = exp( -4 ./ R ); %
    Size ratio of coarse to fine particles
    PE_10(j) = PE_C + ( 1 - PE_C ) .* PE_F .* F3(j) .* F4(j);
end
%%
D_mix = (Xf_max * D_fine + (1 - Xf_max) * D_coarse)';
A1 = [D_mix,D_coarse_name]';
formatSpec = 'Mean Particle Size is %5.2f microns for H%2.0f.\n';
fprintf(formatSpec,A1)
disp(' ')
A2 = [Xf_10;PE_10];
formatSpec2 = 'Xf is %6.2f for a Max Packing Efficiency of %4.2f.\n';
fprintf(formatSpec2,A2)
%%
plot(Xf_10,PE_10,'ko')
```

```

title('Packing Efficiency')
xlabel('Volume Fraction of Fine Particles [Xf]')
ylabel('Relative Packing Density [PE]')
axis([0 1 0.55 0.85])
legend('H3', 'H5', 'H10', 'H15', 'H30', 'H50', 'H60', 'H95', 'PE Max')
grid on
hold off
%% Plot of Diameters vs. Packing Efficiency
figure
plot(D_mix, PE_max, 'r*')
title('PE vs Particle Size')
xlabel('Particel Size [um]')
ylabel('Max Packing Efficiency')

```

B. DENSITY PLOT MATLAB CODES

```
%% Average Density H15 cylinder
```

```

x = [1 2 3]; %sample number
y = [2.63 2.62 2.64]; %g projectile mass
plot(x,y, 'bo')
hold on
lsline
ylim([0 5]) %y-axis range
xlim([0 4]) %y-axis range
legend('H15 CYL', 'Location', 'northoutside')
xlabel('Sample number')
ylabel('Density (g/cc)')

```

```
%% Average Density H15/Sn cylinders
```

```

x = [1 2 3 4 5 6 7 8 9 10 11 12]; %sample number
y = [2.84 2.84 2.83 2.84 2.75 2.82 2.83 2.81 2.79 2.76 2.79 2.80]; %g
projectile mass
plot(x,y, 'bo')
hold on
lsline
ylim([0 4]) %y-axis range
xlim([0 13]) %y-axis range
legend('H15/Sn CYL', 'Location', 'northoutside')
xlabel('Sample number')
ylabel('Density (g/cc)')

```

```
%% Average Density H2/H15 cylinder
```

```

x = [1 2 3 4 5 6 7 8 9 10 11 12]; %sample number
y = [2.61 2.60 2.62 2.57 2.64 2.62 2.62 2.58 2.53 2.55 2.62 2.55]; %g
projectile mass
plot(x,y,'bo')
hold on
lsline
ylim([0 5]) %y-axis range
xlim([0 13]) %y-axis range
legend('H2/H15 CYL','Location','northoutside')
xlabel('Sample number')
ylabel('Density (g/cc)')

```

```

%% Average Density H15 cases

```

```

x = [1 2 3 4 5 6 7 8 9]; %sample number
y = [2.47 2.47 2.44 2.31 2.47 2.35 2.36 2.41 2.52]; %g projectile mass
plot(x,y,'bo')
hold on
lsline
ylim([0 4]) %y-axis range
xlim([0 10]) %y-axis range
legend('H15 cases','Location','northoutside')
xlabel('Sample number')
ylabel('Density (g/cc)')

```

C. STRESS / STRAIN PLOT MATLAB CODES

```

%% Stress vs strain Moderate strain rate 10x10 samples

```

```

close all
clear all
clc

```

```

%load excel data

```

```

data10_10=xlsread('H2_H15_H15_Sn_10_10.xlsx');

```

```

%30psi

```

```

TrueStrainShot1_H2H15=data10_10(:,1);
TrueStressShot1_H2H15=data10_10(:,2);
A1 = smoothdata(TrueStressShot1_H2H15);

```

```

TrueStrainShot1_H15Sn=data10_10(:,10);
TrueStressShot1_H15Sn=data10_10(:,11);
A2 = smoothdata(TrueStressShot1_H15Sn);

```

```

% TrueStrainShot1_H15=dataH15(:,1);
% TrueStressShot1_H15=dataH15(:,2);
% A3 = smoothdata(TrueStressShot1_H15);

```

```

%75psi
TrueStrainShot2_H2H15=data10_10(:,4);
TrueStressShot2_H2H15=data10_10(:,5);
B1 = smoothdata(TrueStressShot2_H2H15);

TrueStrainShot2_H15Sn=data10_10(:,13);
TrueStressShot2_H15Sn=data10_10(:,14);
B2 = smoothdata(TrueStressShot2_H15Sn);

TrueStrainShot2_H15=data10_10(:,19);
TrueStressShot2_H15=data10_10(:,20);
B3 = smoothdata(TrueStressShot2_H15);

%125psi
TrueStrainShot3_H2H15=data10_10(:,7);
TrueStressShot3_H2H15=data10_10(:,8);
C1 = smoothdata(TrueStressShot3_H2H15);

TrueStrainShot3_H15Sn=data10_10(:,16);
TrueStressShot3_H15Sn=data10_10(:,17);
C2 = smoothdata(TrueStressShot3_H15Sn);

% TrueStrainShot3_H15=dataH15(:,7);
% TrueStressShot3_H15=dataH15(:,8);
% C3 = smoothdata(TrueStressShot3_H15);

%Plot 30psi
figure(1)
plot(TrueStrainShot1_H2H15,A1,'b.')
hold on
plot(TrueStrainShot1_H15Sn,A2,'r.')
% plot(TrueStrainShot1_H15,A3,'k.')
hold off
xlim([0 0.065]) %y-axis range
title('L=10mm, D=10mm, Strain Rate = 600s-1')
legend('H2/H15','H15/Sn','Location','south')
xlabel('True Strain (mm)')
ylabel('True Stress (MPa)')

%Plot 75psi
figure(2)
plot(TrueStrainShot2_H2H15,B1,'b.')
hold on
plot(TrueStrainShot2_H15Sn,B2,'r.')
plot(TrueStrainShot2_H15,B3,'k.')
xlim([0 0.14]) %y-axis range
title('L=10mm, D=10mm, Strain Rate = 1200s-1')
legend('H2/H15','H15/Sn','H15','Location','south')
xlabel('True Strain (mm)')
ylabel('True Stress (MPa)')

%Plot 125psi

```

```

figure(3)
plot(TrueStrainShot3_H2H15,C1,'b.')
hold on
plot(TrueStrainShot3_H15Sn,C2,'r.')
% plot(TrueStrainShot3_H15,C3,'k.')
xlim([0 0.2]) %y-axis range
title('L=10mm, D=10mm')
legend('H2/H15, strain rate = 1700s^-^1', 'H15/Sn, strain rate = 1500s^-^1', 'Location', 'south')
xlabel('True Strain (mm)')
ylabel('True Stress (MPa)')

```

```

%% Stress vs strain High strain rate 5x5 samples

```

```

%load excel data
data5_5=xlsread('H2_H15_H15_Sn_5_5.xlsx');
data_H15=xlsread('H15_Data.xlsx');
%30psi
TrueStrainShot1_H2H15=data5_5(:,1);
TrueStressShot1_H2H15=data5_5(:,2);
A1 = smoothdata(TrueStressShot1_H2H15);

TrueStrainShot1_H15Sn=data5_5(:,10);
TrueStressShot1_H15Sn=data5_5(:,11);
A2 = smoothdata(TrueStressShot1_H15Sn);

TrueStrainShot1_H15=data_H15(:,7);
TrueStressShot1_H15=data_H15(:,8);
A3 = smoothdata(smoothdata(TrueStressShot1_H15));

% TrueStrainShot1_H15=dataH15(:,1);
% TrueStressShot1_H15=dataH15(:,2);
% A3 = smoothdata(TrueStressShot1_H15);

%75psi
TrueStrainShot2_H2H15=data5_5(:,4);
TrueStressShot2_H2H15=data5_5(:,5);
B1 = smoothdata(TrueStressShot2_H2H15);

TrueStrainShot2_H15Sn=data5_5(:,13);
TrueStressShot2_H15Sn=data5_5(:,14);
B2 = smoothdata(TrueStressShot2_H15Sn);

% TrueStrainShot2_H15=dataH15(:,4);
% TrueStressShot2_H15=dataH15(:,5);
% B3 = smoothdata(TrueStressShot2_H15);

%125psi
TrueStrainShot3_H2H15=data5_5(:,7);

```

```

TrueStressShot3_H2H15=data5_5(:,8);
C1 = smoothdata(TrueStressShot3_H2H15);

TrueStrainShot3_H15Sn=data5_5(:,16);
TrueStressShot3_H15Sn=data5_5(:,17);
C2 = smoothdata(TrueStressShot3_H15Sn);

% TrueStrainShot3_H15=dataH15(:,7);
% TrueStressShot3_H15=dataH15(:,8);
% C3 = smoothdata(TrueStressShot3_H15);

%Plot 30psi
figure(1)
plot(TrueStrainShot1_H2H15,A1,'b.')
hold on
plot(TrueStrainShot1_H15Sn,A2,'r.')
plot(TrueStrainShot1_H15,A3,'k.')
hold off
xlim([0 0.25]) %y-axis range
title('L=5mm, D=5mm, Strain Rate = 2200s^-1')
legend('H2/H15', 'H15/Sn', 'H15', 'Location', 'south')
xlabel('True Strain (mm)')
ylabel('True Stress (MPa)')

%Plot 75psi
figure(2)
plot(TrueStrainShot2_H2H15,B1,'b.')
hold on
plot(TrueStrainShot2_H15Sn,B2,'r.')
% plot(TrueStrainShot2_H15,B3,'k.')
xlim([0 0.45]) %y-axis range
title('L=5mm, D=5mm, Strain Rate = 3500s^-1')
legend('H2/H15', 'H15/Sn', 'Location', 'south')
xlabel('True Strain (mm)')
ylabel('True Stress (MPa)')

%Plot 125psi
figure(3)
plot(TrueStrainShot3_H2H15,C1,'b.')
hold on
plot(TrueStrainShot3_H15Sn,C2,'r.')
% plot(TrueStrainShot3_H15,C3,'k.')
xlim([0 0.5]) %y-axis range
title('L=5mm, D=5mm, Strain Rate = 4500s^-1')
legend('H2/H15', 'H15/Sn', 'Location', 'south')
xlabel('True Strain (mm)')
ylabel('True Stress (MPa)')

```

D. BRAZILIAN FORCE / STRAIN PLOT MATLAB CODES

```
%% Brazilian test

close all
clear all
clc

%load excel data
data_Brazilian=xlsread('H2_H15_H15_Sn_Brazilian.xlsx');

%Shot_1
TrueStrainShot1_H2H15=data_Brazilian(:,13);
TrueForceShot1_H2H15=data_Brazilian(:,15);
A1 = smoothdata(TrueForceShot1_H2H15);

TrueStrainShot1_H15Sn=data_Brazilian(:,1);
TrueForceShot1_H15Sn=data_Brazilian(:,3);
A2 = smoothdata(TrueForceShot1_H15Sn);

%Shot_2
TrueStrainShot2_H2H15=data_Brazilian(:,17);
TrueForceShot2_H2H15=data_Brazilian(:,19);
B1 = smoothdata(TrueForceShot2_H2H15);

TrueStrainShot2_H15Sn=data_Brazilian(:,5);
TrueForceShot2_H15Sn=data_Brazilian(:,7);
B2 = smoothdata(TrueForceShot2_H15Sn);

%Shot_3
TrueStrainShot3_H2H15=data_Brazilian(:,21);
TrueForceShot3_H2H15=data_Brazilian(:,23);
C1 = smoothdata(TrueForceShot3_H2H15);

TrueStrainShot3_H15Sn=data_Brazilian(:,9);
TrueForceShot3_H15Sn=data_Brazilian(:,11);
C2 = smoothdata(TrueForceShot3_H15Sn);

TrueStrainShot3_H15=data_Brazilian(:,25);
TrueForceShot3_H15=data_Brazilian(:,27);
C3 = smoothdata(TrueForceShot3_H15);

%Plot 1
figure(1)
plot(TrueStrainShot1_H2H15,A1,'b.')
hold on
plot(TrueStrainShot1_H15Sn,A2,'r.')
hold off
xlim([0 0.2]) %y-axis range
title('Brazilian Shot 1')
legend('H2/H15','H15/Sn','Location','south')
```

```

xlabel('True Strain (mm)')
ylabel('Force (N)')

%Plot 2
figure(2)
plot(TrueStrainShot2_H2H15,B1,'b.')
hold on
plot(TrueStrainShot2_H15Sn,B2,'r.')
hold off
xlim([0 0.2]) %y-axis range
title('Brazilian Shot 2')
legend('H2/H15','H15/Sn','Location','south')
xlabel('True Strain (mm)')
ylabel('Force (N)')

%Plot 3
figure(3)
plot(TrueStrainShot3_H2H15,C1,'b.')
hold on
plot(TrueStrainShot3_H15Sn,C2,'r.')
plot(TrueStrainShot3_H15,C3,'k.')
hold off
xlim([0 0.2]) %y-axis range
title('Brazilian Shot 3')
legend('H2/H15','H15/Sn','H15','Location','south')
xlabel('True Strain (mm)')
ylabel('Force (N)')

```

E. PROBABILITY DENSITY FUNCTION AND CUMULATIVE DISTRIBUTION FUNCTION MATLAB CODE

```

%%%%%%%%%%%%%%%%%%%%%%%%%%%%%%%%%%%%%%%%%%%%%%%%%%%%%%%%%%%%%%%%%%%%%%%%
%%%
% CamSizer.m
% Fit data from the Haver-Tyler optical size analyzer ("camsizer")
using a
% bimodel three-dimensional Mott distribution converted to mass
distributed
% over a linear size.
%
% Excel files should have the following columns:
% Midpoint | Retaining Count (1-Q0) | Density (Count) | Retaining
volume
% (1-Q3) | Density (Volume)
%
%%%%%%%%%%%%%%%%%%%%%%%%%%%%%%%%%%%%%%%%%%%%%%%%%%%%%%%%%%%%%%%%%%%%%%%%
%%%
clear all;
close all;
%%%%%%%%%%%%%%%%%%%%%%%%%%%%%%%%%%%%%%%%%%%%%%%%%%%%%%%%%%%%%%%%%%%%%%%%

```

```

% Fit functions
%%%%%%%%%%%%%%%%%%%%%%%%%%%%%%%%%%%%%%%%%%%%%%%%%%%%%%%%%%%%%%%%%%%%%%%%
% 3d Mott forms
mcdf=@(fitVals,sdata)1-exp(-
sdata./fitVals(1)).*(1+sdata./fitVals(1)+...

0.5*(sdata.^2)./(fitVals(1).^2)+(1.0/6.0).*(sdata.^3)./(fitVals(1).^3))
;
mpdf=@(fitVals,sdata)(1./(6.0.*fitVals(1))).*((sdata./fitVals(1)).^3.0)
.*...
    exp(-sdata./fitVals(1));

%Updated mass pdf for 0 minute shots
mpdf0min=@(fitVals,sdata)fitVals(1).*(exp(-1.*fitVals(1).*(sdata-
0.044)));
mcdf0min=@(fitVals,sdata)(1-exp(-1.*fitVals(1).*(sdata-0.044)));

% Bimodal forms
bimodalmpdf=@(fitVals,sdata)fitVals(1).*mpdf(fitVals(2),sdata)+...
    (1.0-fitVals(1)).*mpdf(fitVals(3),sdata);
bimodalmcdf=@(fitVals,sdata)fitVals(1).*mcdf(fitVals(2),sdata)+...
    (1.0-fitVals(1)).*mcdf(fitVals(3),sdata);

bimodalMottPowerlawPDF=@(fitVals,sdata)fitVals(1).*fitVals(2).*(exp(-
1.*fitVals(2).*(sdata-0.044)))+...
    (1-
fitVals(1)).*(1./(6.0.*fitVals(3))).*((sdata)./fitVals(3)).^3.0).*...
    exp(-(sdata)./fitVals(3));

bimodalMottPowerlawCDF=@(fitVals,sdata)fitVals(1).*(1-exp(-
fitVals(2).*(sdata-0.044)))+...
    (1-fitVals(1)).*(1-exp(-
(sdata)./fitVals(3)).*(1+(sdata)./fitVals(3)+...

0.5*(((sdata).^2)./(fitVals(3)).^2)+(1.0/6.0).*((sdata).^3)./(fitVals(
3)).^3)));

%%%%%%%%%%%%%%%%%%%%%%%%%%%%%%%%%%%%%%%%%%%%%%%%%%%%%%%%%%%%%%%%%%%%%%%%
% Excel data files
%%%%%%%%%%%%%%%%%%%%%%%%%%%%%%%%%%%%%%%%%%%%%%%%%%%%%%%%%%%%%%%%%%%%%%%%

% input file
dataPureH15=xlsread('PureH15.xlsx');
dataH15H2=xlsread('H15H2.xlsx');
dataH15Sn10=xlsread('H15Sn10.xlsx');

% Pure H15 - Shots 1 to 3
midpointsPureH15Shot1=dataPureH15(:,1);
cdfCountPureH15Shot1=1.0-dataPureH15(:,2)./100;
pdfCountPureH15Shot1=dataPureH15(:,3)./100;
cdfVolPureH15Shot1=(1.0-dataPureH15(:,4)./100);
pdfVolPureH15Shot1=dataPureH15(:,5)./100;

```

```

midpointsPureH15Shot2=dataPureH15(:,1);
cdfCountPureH15Shot2=1.0-dataPureH15(:,6)./100;
pdfCountPureH15Shot2=dataPureH15(:,7)./100;
cdfVolPureH15Shot2=(1.0-dataPureH15(:,8)./100);
pdfVolPureH15Shot2=dataPureH15(:,9)./100;

midpointsPureH15Shot3=dataPureH15(:,1);
cdfCountPureH15Shot3=1.0-dataPureH15(:,10)./100;
pdfCountPureH15Shot3=dataPureH15(:,11)./100;
cdfVolPureH15Shot3=(1.0-dataPureH15(:,12)./100);
pdfVolPureH15Shot3=dataPureH15(:,13)./100;

% H15 H2 - Shots 1 to 2
midpointsH15H2Shot1=dataH15H2(:,1);
cdfCountH15H2Shot1=1.0-dataH15H2(:,2)./100;
pdfCountH15H2Shot1=dataH15H2(:,3)./100;
cdfVolH15H2Shot1=(1.0-dataH15H2(:,4)./100);
pdfVolH15H2Shot1=dataH15H2(:,5)./100;

midpointsH15H2Shot2=dataH15H2(:,1);
cdfCountH15H2Shot2=1.0-dataH15H2(:,6)./100;
pdfCountH15H2Shot2=dataH15H2(:,7)./100;
cdfVolH15H2Shot2=(1.0-dataH15H2(:,8)./100);
pdfVolH15H2Shot2=dataH15H2(:,9)./100;

% H15 Sn10 - Shots 1 to 3
midpointsH15Sn10Shot1=dataH15Sn10(:,1);
cdfCountH15Sn10Shot1=1.0-dataH15Sn10(:,2)./100;
pdfCountH15Sn10Shot1=dataH15Sn10(:,3)./100;
cdfVolH15Sn10Shot1=(1.0-dataH15Sn10(:,4)./100);
pdfVolH15Sn10Shot1=dataH15Sn10(:,5)./100;

midpointsH15Sn10Shot2=dataH15Sn10(:,1);
cdfCountH15Sn10Shot2=1.0-dataH15Sn10(:,6)./100;
pdfCountH15Sn10Shot2=dataH15Sn10(:,7)./100;
cdfVolH15Sn10Shot2=(1.0-dataH15Sn10(:,8)./100);
pdfVolH15Sn10Shot2=dataH15Sn10(:,9)./100;

midpointsH15Sn10Shot3=dataH15Sn10(:,1);
cdfCountH15Sn10Shot3=1.0-dataH15Sn10(:,10)./100;
pdfCountH15Sn10Shot3=dataH15Sn10(:,11)./100;
cdfVolH15Sn10Shot3=(1.0-dataH15Sn10(:,12)./100);
pdfVolH15Sn10Shot3=dataH15Sn10(:,13)./100;

%%%%%%%%%%%%%%%%%%%%%%%%%%%%%%%%%%%%%%%%%%%%%%%%%%%%%%%%%%%%%%%%%%%%%%%%
% Fit to mass PDF
%%%%%%%%%%%%%%%%%%%%%%%%%%%%%%%%%%%%%%%%%%%%%%%%%%%%%%%%%%%%%%%%%%%%%%%%
lowerBound=[0.0 1e-5 0.1];
upperBound=[1.0 2.0 10.0];
guess=[0.1 0.2 1.0];
dim=[0.15 0.7 0.2 0.2];

```

```

% Set to 1 to use a bimodal fit. 0 for unimodal.

useBimodal=1;

if useBimodal==0
    guess=1.0;

[fitValsMassPDFPureH15Shot1, resnorm]=lsqcurvefit(mcdf, guess, midpointsPureH15Shot1, cdfVolPureH15Shot1, lowerBound, upperBound);

[fitValsMassPDFPureH15Shot2, resnorm]=lsqcurvefit(mcdf, guess, midpointsPureH15Shot2, cdfVolPureH15Shot2, lowerBound, upperBound);

[fitValsMassPDFPureH15Shot3, resnorm]=lsqcurvefit(mcdf, guess, midpointsPureH15Shot3, cdfVolPureH15Shot3, lowerBound, upperBound);

[fitValsMassPDFH15H2Shot1, resnorm]=lsqcurvefit(mcdf, guess, midpointsH15H2Shot1, cdfVolH15H2Shot1, lowerBound, upperBound);

[fitValsMassPDFH15H2Shot2, resnorm]=lsqcurvefit(mcdf, guess, midpointsH15H2Shot2, cdfVolH15H2Shot2, lowerBound, upperBound);

[fitValsMassPDFH15Sn10Shot1, resnorm]=lsqcurvefit(mcdf, guess, midpointsH15Sn10Shot1, cdfVolH15Sn10Shot1, lowerBound, upperBound);

[fitValsMassPDFH15Sn10Shot2, resnorm]=lsqcurvefit(mcdf, guess, midpointsH15Sn10Shot2, cdfVolH15Sn10Shot2, lowerBound, upperBound);

[fitValsMassPDFH15Sn10Shot3, resnorm]=lsqcurvefit(mcdf, guess, midpointsH15Sn10Shot3, cdfVolH15Sn10Shot3, lowerBound, upperBound);

    denseSSpace=linspace(0, 11, 10000);

theoryCurvePureH15Shot1=mpdf(fitValsMassPDFPureH15Shot1, denseSSpace);

theoryCurvePureH15Shot2=mpdf(fitValsMassPDFPureH15Shot2, denseSSpace);

theoryCurvePureH15Shot3=mpdf(fitValsMassPDFPureH15Shot3, denseSSpace);
    theoryCurveH15H2Shot1=mpdf(fitValsMassPDFH15H2Shot1, denseSSpace);
    theoryCurveH15H2Shot2=mpdf(fitValsMassPDFH15H2Shot2, denseSSpace);

theoryCurveH15Sn10Shot1=mpdf(fitValsMassPDFH15Sn10Shot1, denseSSpace);

theoryCurveH15Sn10Shot2=mpdf(fitValsMassPDFH15Sn10Shot2, denseSSpace);

theoryCurveH15Sn10Shot3=mpdf(fitValsMassPDFH15Sn10Shot3, denseSSpace);
end

if useBimodal==1

```

```

[fitValsMassPDFPureH15Shot1, resnorm]=lsqcurvefit(bimodalMottPowerlawPDF
,guess,midpointsPureH15Shot1,pdfVolPureH15Shot1,lowerBound,upperBound);
[fitValsMassPDFPureH15Shot2, resnorm]=lsqcurvefit(bimodalMottPowerlawPDF
,guess,midpointsPureH15Shot2,pdfVolPureH15Shot2,lowerBound,upperBound);
[fitValsMassPDFPureH15Shot3, resnorm]=lsqcurvefit(bimodalMottPowerlawPDF
,guess,midpointsPureH15Shot3,pdfVolPureH15Shot3,lowerBound,upperBound);
[fitValsMassPDFH15H2Shot1, resnorm]=lsqcurvefit(bimodalMottPowerlawPDF,g
uess,midpointsH15H2Shot1,pdfVolH15H2Shot1,lowerBound,upperBound);
[fitValsMassPDFH15H2Shot2, resnorm]=lsqcurvefit(bimodalMottPowerlawPDF,g
uess,midpointsH15H2Shot2,pdfVolH15H2Shot2,lowerBound,upperBound);
[fitValsMassPDFH15Sn10Shot1, resnorm]=lsqcurvefit(bimodalMottPowerlawPDF
,guess,midpointsH15Sn10Shot1,pdfVolH15Sn10Shot1,lowerBound,upperBound);
[fitValsMassPDFH15Sn10Shot2, resnorm]=lsqcurvefit(bimodalMottPowerlawPDF
,guess,midpointsH15Sn10Shot2,pdfVolH15Sn10Shot2,lowerBound,upperBound);
[fitValsMassPDFH15Sn10Shot3, resnorm]=lsqcurvefit(bimodalMottPowerlawPDF
,guess,midpointsH15Sn10Shot3,pdfVolH15Sn10Shot3,lowerBound,upperBound);

denseSSpace=linspace(0,11,10000);
theoryCurvePureH15Shot1=bimodalMottPowerlawPDF(fitValsMassPDFPureH15Sho
t1,denseSSpace);
theoryCurvePureH15Shot2=bimodalMottPowerlawPDF(fitValsMassPDFPureH15Sho
t2,denseSSpace);
theoryCurvePureH15Shot3=bimodalMottPowerlawPDF(fitValsMassPDFPureH15Sho
t3,denseSSpace);
theoryCurveH15H2Shot1=bimodalMottPowerlawPDF(fitValsMassPDFH15H2Shot1,d
enseSSpace);
theoryCurveH15H2Shot2=bimodalMottPowerlawPDF(fitValsMassPDFH15H2Shot2,d
enseSSpace);
theoryCurveH15Sn10Shot1=bimodalMottPowerlawPDF(fitValsMassPDFH15Sn10Sho
t1,denseSSpace);
theoryCurveH15Sn10Shot2=bimodalMottPowerlawPDF(fitValsMassPDFH15Sn10Sho
t2,denseSSpace);
theoryCurveH15Sn10Shot3=bimodalMottPowerlawPDF(fitValsMassPDFH15Sn10Sho
t3,denseSSpace);

end

%PDF - Pure H15
figure(1)
subplot(1,2,1)
plot(midpointsPureH15Shot1,pdfVolPureH15Shot1,'ok','LineWidth',
2.0,'MarkerSize',8.0);
hold on;
plot(midpointsPureH15Shot2,pdfVolPureH15Shot2,'or','LineWidth',
2.0,'MarkerSize',8.0);
plot(midpointsPureH15Shot3,pdfVolPureH15Shot3,'ob','LineWidth',
2.0,'MarkerSize',8.0);
plot(denseSSpace,theoryCurvePureH15Shot1,'-k','LineWidth',3.0);
plot(denseSSpace,theoryCurvePureH15Shot2,'-r','LineWidth',3.0);
plot(denseSSpace,theoryCurvePureH15Shot3,'-b','LineWidth',3.0);
axis([0 10 0 1]);
%title('Pure H15 - PDF');
xlabel('Size (mm)', 'FontName', 'Times New Roman', 'FontSize', 40);

```

```

ylabel('Mass PDF', 'FontName', 'Times New Roman', 'FontSize', 40);
set(gca, 'FontName', 'Times New Roman', 'FontSize',
18, 'box', 'on', 'LineWidth', 1.1);
legend('Pure H15: v_o=517 m/s (tilted)', 'v_o=627 m/s', 'v_o=565
m/s', 'Box', 'off', 'FontSize', 14, 'Location', 'northeast');

%CDF - Pure H15
%figure(2)
subplot(1,2,2)
plot(midpointsPureH15Shot1, cdfVolPureH15Shot1, 'ok', 'LineWidth',
2.0, 'MarkerSize', 8.0);
hold on;
plot(midpointsPureH15Shot2, cdfVolPureH15Shot2, 'or', 'LineWidth',
2.0, 'MarkerSize', 8.0);
plot(midpointsPureH15Shot3, cdfVolPureH15Shot3, 'ob', 'LineWidth',
2.0, 'MarkerSize', 8.0);
plot(denseSSpace, bimodalMottPowerlawCDF(fitValsMassPDFPureH15Shot1, dens
eSSpace), '-k', 'LineWidth', 3.0);
plot(denseSSpace, bimodalMottPowerlawCDF(fitValsMassPDFPureH15Shot2, dens
eSSpace), '-r', 'LineWidth', 3.0);
plot(denseSSpace, bimodalMottPowerlawCDF(fitValsMassPDFPureH15Shot3, dens
eSSpace), '-b', 'LineWidth', 3.0);
axis([0 10 0 2]);
%title('Pure H15 - CDF');
xlabel('Size (mm)', 'FontName', 'Times New Roman', 'FontSize', 40);
ylabel('Mass CDF', 'FontName', 'Times New Roman', 'FontSize', 40);
set(gca, 'FontName', 'Times New Roman', 'FontSize',
18, 'box', 'on', 'LineWidth', 1.1);
legend('Pure H15: v_o=517 m/s (tilted)', 'v_o=627 m/s', 'v_o=565
m/s', 'Box', 'off', 'FontSize', 14, 'Location', 'northeast');

%PDF - H15/H2
figure(3)
subplot(1,2,1)
plot(midpointsH15H2Shot1, pdfVolH15H2Shot1, 'ok', 'LineWidth',
2.0, 'MarkerSize', 8.0);
hold on;
plot(midpointsH15H2Shot2, pdfVolH15H2Shot2, 'or', 'LineWidth',
2.0, 'MarkerSize', 8.0);
plot(denseSSpace, theoryCurveH15H2Shot1, '-k', 'LineWidth', 3.0);
plot(denseSSpace, theoryCurveH15H2Shot2, '-r', 'LineWidth', 3.0);
axis([0 10 0 1]);
%title('H15/H2 - PDF');
xlabel('Size (mm)', 'FontName', 'Times New Roman', 'FontSize', 40);
ylabel('Mass PDF', 'FontName', 'Times New Roman', 'FontSize', 40);
set(gca, 'FontName', 'Times New Roman', 'FontSize',
18, 'box', 'on', 'LineWidth', 1.1);
legend('H15/H2: v_o=886 m/s', 'v_o=563
m/s', 'Box', 'off', 'FontSize', 14, 'Location', 'northeast');

```

```

%CDF - H15/H2
%figure(4)
subplot(1,2,2)
plot(midpointsH15H2Shot1,cdfVolH15H2Shot1,'ok','LineWidth',
2.0,'MarkerSize',8.0);
hold on;
plot(midpointsH15H2Shot2,cdfVolH15H2Shot2,'or','LineWidth',
2.0,'MarkerSize',8.0);
plot(denseSSpace,bimodalMottPowerlawCDF(fitValsMassPDFH15H2Shot1,denseS
Space),'-k','LineWidth',3.0);
plot(denseSSpace,bimodalMottPowerlawCDF(fitValsMassPDFH15H2Shot2,denseS
Space),'-r','LineWidth',3.0);
axis([0 10 0 2]);
%title('H15/H2 - CDF');
xlabel('Size (mm)', 'FontName', 'Times New Roman', 'FontSize', 40);
ylabel('Mass CDF', 'FontName', 'Times New Roman', 'FontSize', 40);
set(gca,'FontName', 'Times New Roman', 'FontSize',
18,'box','on','LineWidth', 1.1);
legend('H15/H2: v_o=886 m/s','v_o=563
m/s','Box','off','FontSize',14,'Location','northeast');

```

```

%PDF - H15Sn10
figure(5)
subplot(1,2,1)
plot(midpointsH15Sn10Shot1,pdfVolH15Sn10Shot1,'ok','LineWidth',
2.0,'MarkerSize',8.0);
hold on;
plot(midpointsH15Sn10Shot2,pdfVolH15Sn10Shot2,'or','LineWidth',
2.0,'MarkerSize',8.0);
plot(midpointsH15Sn10Shot3,pdfVolH15Sn10Shot3,'ob','LineWidth',
2.0,'MarkerSize',8.0);
plot(denseSSpace,theoryCurveH15Sn10Shot1,'-k','LineWidth',3.0);
plot(denseSSpace,theoryCurveH15Sn10Shot2,'-r','LineWidth',3.0);
plot(denseSSpace,theoryCurveH15Sn10Shot3,'-b','LineWidth',3.0);
axis([0 10 0 1]);
%title('H15/10Sn - PDF');
xlabel('Size (mm)', 'FontName', 'Times New Roman', 'FontSize', 40);
ylabel('Mass PDF', 'FontName', 'Times New Roman', 'FontSize', 40);
set(gca,'FontName', 'Times New Roman', 'FontSize',
18,'box','on','LineWidth', 1.1);
legend('H15/Sn10: v_o=620 m/s','v_o=550 m/s','v_o=518
m/s','Box','off','FontSize',14,'Location','northeast');

```

```

%CDF - H15Sn10
%figure(6)
subplot(1,2,2)
plot(midpointsH15Sn10Shot3,cdfVolH15Sn10Shot3,'ob','LineWidth',
2.0,'MarkerSize',8.0);
hold on;
plot(midpointsH15Sn10Shot1,cdfVolH15Sn10Shot1,'ok','LineWidth',
2.0,'MarkerSize',8.0);

```

```

plot(midpointsH15Sn10Shot2,cdfVolH15Sn10Shot2,'or','LineWidth',
2.0,'MarkerSize',8.0);

plot(denseSSpace,bimodalMottPowerlawCDF(fitValsMassPDFH15Sn10Shot3,dens
eSSpace),'-b','LineWidth',3.0);
plot(denseSSpace,bimodalMottPowerlawCDF(fitValsMassPDFH15Sn10Shot1,dens
eSSpace),'-k','LineWidth',3.0);
plot(denseSSpace,bimodalMottPowerlawCDF(fitValsMassPDFH15Sn10Shot2,dens
eSSpace),'-r','LineWidth',3.0);

axis([0 10 0 2]);
%title('H15/10Sn - CDF');
xlabel('Size (mm)', 'FontName', 'Times New Roman', 'FontSize', 40);
ylabel('Mass CDF', 'FontName', 'Times New Roman', 'FontSize', 40);
set(gca,'FontName', 'Times New Roman', 'FontSize',
18,'box','on','LineWidth', 1.1);
legend('H15/Sn10: v_o=620 m/s','v_o=550 m/s','v_o=518
m/s','Box','off','FontSize',14,'Location','northeast');

% Figure comparing the different materials at a similar velocity
% H15: 565 m/s.
% H15/H2: 563 m/s
% H15/Sn: 550 m/s
figure(7)
plot(midpointsPureH15Shot3,cdfVolPureH15Shot3,'ob','LineWidth',
2.0,'MarkerSize',8.0);
hold on;
plot(midpointsH15H2Shot2,cdfVolH15H2Shot2,'or','LineWidth',
2.0,'MarkerSize',8.0);
plot(midpointsH15Sn10Shot1,cdfVolH15Sn10Shot1,'ok','LineWidth',
2.0,'MarkerSize',8.0);
plot(denseSSpace,bimodalMottPowerlawCDF(fitValsMassPDFPureH15Shot3,dens
eSSpace),'-b','LineWidth',3.0);
plot(denseSSpace,bimodalMottPowerlawCDF(fitValsMassPDFH15H2Shot2,denseS
Space),'-r','LineWidth',3.0);
plot(denseSSpace,bimodalMottPowerlawCDF(fitValsMassPDFH15Sn10Shot1,dens
eSSpace),'-k','LineWidth',3.0);
axis([0 10 0 1.1]);
xlabel('Size (mm)', 'FontName', 'Times New Roman', 'FontSize', 40);
ylabel('Mass CDF', 'FontName', 'Times New Roman', 'FontSize', 40);
set(gca,'FontName', 'Times New Roman', 'FontSize',
18,'box','on','LineWidth', 1.1);
legend('H15: v_o=565 m/s','H15/H2: v_o=563 m/s','H15Sn10: v_o=550
m/s','Box','off','FontSize',16,'Location','southeast');

```

THIS PAGE INTENTIONALLY LEFT BLANK

LIST OF REFERENCES

- [1] Y. Bai, G. Wagner, and C. B Williams, “Effect of Bimodal Powder Packing Density and Sintered Density in Binder Jetting of Metals,” in *Proceeding of Solid Freeform Fabrication (SFF) Symposium*, 2015, pp. 758-771.
- [2] J. Zheng, W. B. Carlson, and J. S. Reed, “The packing density of binary powder mixtures,” in *Journal of the European Ceramic Society*, Vol. 15, 1995.
- [3] D. J. Frew, M. J. Forrestal, and W. Chen, “Pulse Shaping Techniques for Testing Brittle Materials with a Split Hopkinson Pressure Bar,” in *Experimental Mechanics*, Vol. 42, March 2002.
- [4] P. L. Stewart, “Ballistics and fragmentation of the M7 reactive material against oblique targets,” M.S. thesis, Dept. of Eng. and App. Sci., NPS, Monterey, CA, USA, 2017.
- [5] T. A. Booth-Seay, “Soft catch and fragmentation of Navy reactive materials,” M.S. thesis, Dept. of Eng. and App. Sci., NPS, Monterey, CA, USA, 2017.
- [6] D. Li and L. N. Y. Wong, “The Brazilian Disc Test for Rock Mechanics Applications: Review and New Insights,” in *Rock Mechanics and Rock Engineering*, March 2012.
- [7] “Lame parameters,” *Wikipedia*. Accessed November 17, 2018. [online]. Available: https://en.wikipedia.org/wiki/Lamé_parameters

THIS PAGE INTENTIONALLY LEFT BLANK

INITIAL DISTRIBUTION LIST

1. Defense Technical Information Center
Ft. Belvoir, Virginia
2. Dudley Knox Library
Naval Postgraduate School
Monterey, California